AGU PUBLICATIONS

JGR

Journal of Geophysical Research: Atmospheres

RESEARCH ARTICLE
10.1002/2014JD022732

Key Points:
- Interferences contribute on average 22% of PTR-MS m/z 69 signal
- Isoprene emissions are underestimated in the US Upper Midwest
- Spatiotemporal distribution of isoprene emissions drives NO_x-VOC chemical shifts

Supporting Information:
- Tables S1–S3 and Figure S1

Correspondence to:
D. B. Millet,
dbm@umn.edu

Citation:
Hu, L., D. B. Millet, M. Baasandorj, T. J. Griffis, P. Turner, D. Helmig, A. J. Curtis, and J. Hueber (2015), Isoprene emissions and impacts over an ecological transition region in the U.S. Upper Midwest inferred from tall tower measurements, *J. Geophys. Res. Atmos.*, *120*, 3553–3571, doi:10.1002/2014JD022732.

Received 16 OCT 2014
Accepted 15 MAR 2015
Accepted article online 19 MAR 2015
Published online 24 APR 2015

Isoprene emissions and impacts over an ecological transition region in the U.S. Upper Midwest inferred from tall tower measurements

Lu Hu[1,2], Dylan B. Millet[1], Munkhbayar Baasandorj[1], Timothy J. Griffis[1], Peter Turner[1], Detlev Helmig[3], Abigale J. Curtis[3], and Jacques Hueber[3]

[1]Department of Soil, Water, and Climate, University of Minnesota, St. Paul, Minnesota, USA, [2]School of Engineering and Applied Sciences, Harvard University, Cambridge, Massachusetts, USA, [3]Institute of Arctic and Alpine Research, University of Colorado, Boulder, Colorado, USA

Abstract We present 1 year of in situ proton transfer reaction mass spectrometer (PTR-MS) measurements of isoprene and its oxidation products methyl vinyl ketone (MVK) and methacrolein (MACR) from a 244 m tall tower in the U.S. Upper Midwest, located at an ecological transition between isoprene-emitting deciduous forest and predominantly non-isoprene-emitting agricultural landscapes. We find that anthropogenic interferences (or anthropogenic isoprene) contribute on average 22% of the PTR-MS *m/z* 69 signal during summer daytime, whereas MVK + MACR interferences (*m/z* 71) are minor (7%). After removing these interferences, the observed isoprene and MVK + MACR abundances show pronounced seasonal cycles, reaching summertime maxima of >2500 pptv (1 h mean). The tall tower is impacted both by nearby and more distant regional isoprene sources, with daytime enhancements of isoprene (but little MVK + MACR) under southwest winds and enhancements of MVK + MACR (but little isoprene) at other times. We find that the GEOS-Chem atmospheric model with the MEGANv2.1 (Model of Emissions of Gases and Aerosols from Nature version 2.1) biogenic inventory can reproduce the isoprene observations to within model uncertainty given improved land cover and temperature estimates. However, a 60% low model bias in MVK + MACR cannot be resolved, even across diverse model assumptions for NO_x emissions, chemistry, atmospheric mixing, dry deposition, land cover, and potential measurement interferences. This implies that, while isoprene emissions in the immediate vicinity of the tall tower are adequately captured, they are underestimated across the broader region. We show that this region experiences a strong seasonal shift between VOC-limited chemistry during the spring and fall and NO_x-limited or transitional chemistry during the summer, driven by the spatiotemporal distribution of isoprene emissions. Isoprene's role in causing these chemical shifts is likely underestimated due to the underprediction of its regional emissions.

1. Introduction

Biogenic volatile organic compounds (BVOCs) play a major role in atmospheric chemistry and climate. They are precursors of ozone and of secondary organic aerosol, and modulate the troposphere's oxidizing potential and thus the lifetime of methane and other greenhouse gases and pollutants. Of the more than 1000 VOCs that have been measured in the atmosphere [*Goldstein and Galbally*, 2007], the estimated global emissions of isoprene (2-methyl-1,3-butadiene, C_5H_8) are (i) believed to account for some ~50% of the total BVOC flux each year [*Guenther et al.*, 2006], (ii) comparable to those of methane [*Chen and Prinn*, 2006], and (iii) several times larger than those of all anthropogenic VOCs combined [*Guenther et al.*, 2012; *Hu et al.*, 2015].

Isoprene is produced enzymatically in the foliage of terrestrial plants, and the resulting emissions can account for 0.1–3% of annual net photosynthetic carbon uptake for certain plant species [*Sharkey et al.*, 1996; *Goldstein et al.*, 1998]. Isoprene emission may have evolved in plants as a mechanism for coping with heat stress [*Sasaki et al.*, 2007; *Sharkey et al.*, 2008], although other adaptive benefits have also been proposed [*Monson et al.*, 2013]. Emissions vary between species and depend strongly on temperature and light, as well as on other environmental and ecological factors such as soil moisture, phenology, nutrient availability, and atmospheric CO_2 concentration [*Sharkey et al.*, 1991; *Goldstein et al.*, 1998; *Harley et al.*, 1999; *Guenther et al.*, 2012; *Monson et al.*, 2012]. Isoprene is highly reactive in the atmosphere, with a lifetime against oxidation by the hydroxyl radical (OH) of about 1 h during daytime in summer (82 min for an assumed $[OH] = 2 \times 10^6$ molecules cm^{-3})

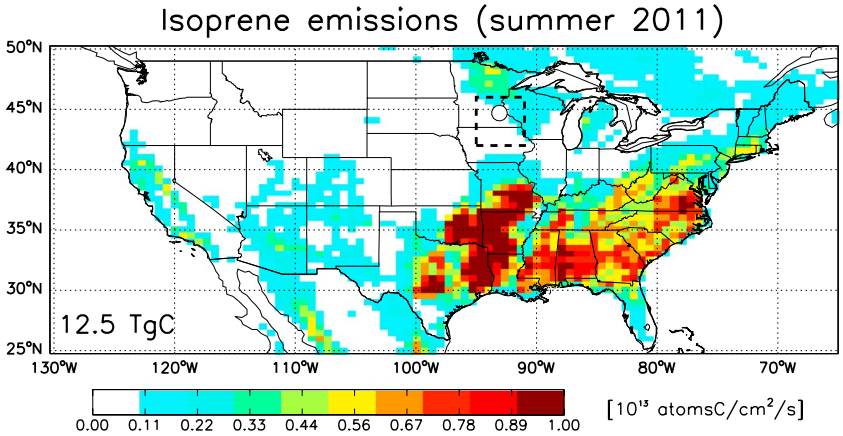

Figure 1. Isoprene emissions during summer (June–August) 2011 computed based on MEGANv2.1 with GEOS-5.2 assimilated meteorological data and CLM4 land cover data as inputs (see text). The total predicted isoprene flux over the domain and time frame of the figure is given inset. The KCMP tall tower location is indicated by the circle, while the dashed box indicates the Upper Midwest region displayed in subsequent figures.

[*Atkinson et al.*, 2006]; first-generation oxidation products include methyl vinyl ketone (MVK), methacrolein (MACR), formaldehyde, hydroxyhydroperoxides, hydroperoxyaldehydes, and isoprene nitrates [*Pierotti et al.*, 1990; *Montzka et al.*, 1993; *Warneke et al.*, 2001; *Paulot et al.*, 2009b; *Crounse et al.*, 2011].

Global isoprene emissions are currently estimated at 350–800 Tg yr^{-1} [*Arneth et al.*, 2008; *Guenther et al.*, 2012]. Bottom-up emission uncertainties are typically estimated at a factor of 2 or more, based on top-down information from satellite-based measurements of formaldehyde columns [*Palmer et al.*, 2003; *Shim et al.*, 2005; *Fu et al.*, 2007; *Millet et al.*, 2008; *Barkley et al.*, 2011; *Marais et al.*, 2012, 2014] and aircraft observations [*Karl et al.*, 2007; *Warneke et al.*, 2010; *Misztal et al.*, 2014]. Errors on local-to-regional scales are often even larger [*Guenther et al.*, 2006, 2012]. Predicted isoprene fluxes are highly dependent on model inputs such as weather, leaf area index (LAI), and land cover [*Sharkey et al.*, 1996; *Arneth et al.*, 2008]; and as a result, it is often a major challenge to discern whether discrepancies between an emission inventory and observations arise from unrealistic inputs used to drive the emission models or from the emission model algorithms themselves [*Lamb et al.*, 1987; *Guenther et al.*, 2012].

Prior evaluations of isoprene emission estimates over North America have led to seemingly inconsistent conclusions. For example, the total North American isoprene flux derived from formaldehyde column measurements from three different satellite sensors (Ozone Monitoring Instrument (OMI), Global Ozone Monitoring Experiment (GOME), and Scanning Imaging Absorption Spectrometer for Atmospheric Chartography (SCIAMACHY)) was found to be 4–40% lower than predicted by MEGANv2 (Model of Emissions of Gases and Aerosols from Nature version 2) [*Palmer et al.*, 2006; *Millet et al.*, 2008; *Stavrakou et al.*, 2009], with a somewhat larger bias over the U.S. Upper Midwest (~70%) [*Millet et al.*, 2008]. A subsequent analysis of airborne measurements suggested that MEGANv2 overpredicts isoprene emissions over the eastern United States and Texas by up to a factor of 2 [*Warneke et al.*, 2010]. On the other hand, *Müller et al.* [2008] found that isoprene emissions predicted on the basis of MEGANv2 and a detailed canopy environment model were 40% too low compared to in situ flux measurements at Harvard Forest in central Massachusetts, USA, a site with 60–70% broadleaf deciduous tree coverage [*Goldstein et al.*, 1998]. However, the above studies employed divergent meteorological and land cover data sets, and differed also in their implementation of MEGAN within the overarching chemical transport model or CTM (e.g., in the parameterization of the forest canopy). Collective interpretation of such studies in terms of broader implications for emission models such as MEGAN, therefore, requires careful consideration of how the overall CTM framework and driving variables affect the emission estimates.

In this study, we present a full year of continuous in situ concentration measurements of isoprene and its oxidation products (MVK + MACR) from a tall tower in the U.S. Upper Midwest (KCMP tall tower; Figure 1). The site is ~25 km south of the Twin Cities (Minneapolis and St. Paul) and lies at the ecological transition between high-isoprene-emitting eastern deciduous forest to the north and east, and predominantly non-isoprene-emitting agricultural landscapes to the west and south (Figures 1 and 2). We interpret this data set with a

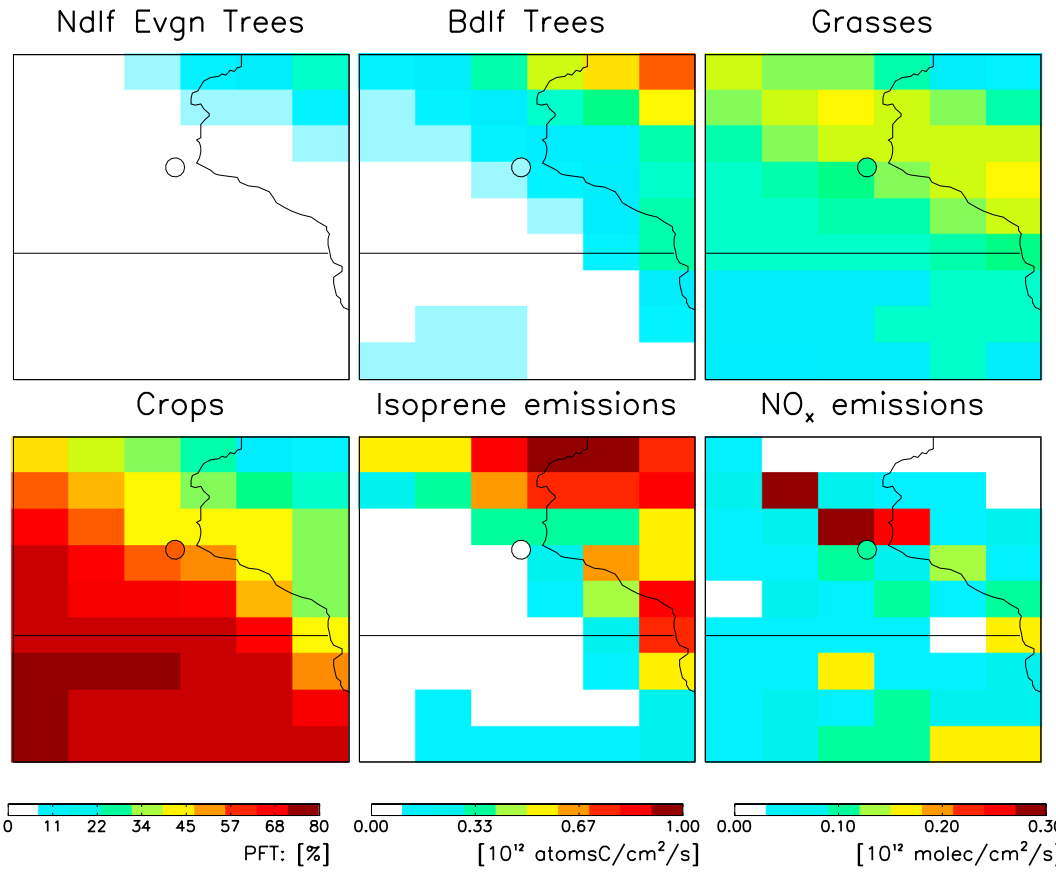

Figure 2. Fractional distribution of major plant functional types in the vicinity of the KCMP tall tower, according to CLM4 (year 2005): Ndlf Evgn Trees = needleleaf evergreen trees, Bdlf Trees = broadleaf trees, grasses, and crops. Also shown are the simulated isoprene emissions and NO_x emissions (summer monthly mean) for 2011. See text for details. The location of the KCMP tall tower is indicated by the filled circle, and the figure domain corresponds to the dashed rectangle in Figure 1. The Twin Cities of Minneapolis and Saint Paul are located ~30–40 km northwest and north of the tower location.

0.5° × 0.667° (latitude × longitude) nested version of the GEOS-Chem CTM in terms of its implications for present understanding of isoprene emissions and chemical impact in this region. We further investigate the role of isoprene in driving a seasonal shift between NO_x- and VOC-limited photochemistry during the spring and fall in this part of the U.S. Upper Midwest.

2. Methods

2.1. KCMP Tall Tower

Figure 2 shows the fractional distributions of four major plant functional types (PFTs) in the U.S. Upper Midwest [*Oleson et al.*, 2010], along with annual isoprene and NO_x emissions for this region computed as described in section 2.3. As we see, the KCMP tall tower (and the nearby Twin Cities) is situated on a strong isoprene emission gradient between the deciduous forests to the northeast and mainly agricultural areas to the southwest. The tower is also at times downwind of the Twin Cities (2010 metropolitan statistical area population: 3.3 M; http://www.census.gov/compendia/statab/2012/tables/12s0020.xls) and, therefore, is periodically impacted by urban pollution outflow. The tower location thus provides a unique natural laboratory to study interacting biogenic and anthropogenic processes. A detailed description of the KCMP tall tower and of the meteorological measurements at the site is given in earlier papers [*Griffis et al.*, 2010; *Hu et al.*, 2011].

2.2. PTR-MS and Cartridge-GC-MS/FID Measurements at the KCMP Tall Tower

Isoprene (protonated *m/z* 69), its oxidation products MVK + MACR (protonated *m/z* 71), and a suite of other VOCs (including methanol, acetone, acetonitrile, and C_6–C_9 aromatic compounds) were measured using

Table 1. Mixing Ratios of the Primary VOC Calibration Standards (in ppbv) Over the Course of the Study Period Relative to the Original Certified Values

	Original[a]	Cartridge-GC-MS/FID[b]				Reanalysis[a]
Date	12/2008	12/2010	4/2011	4/2011	7/2011	1/2012
Isoprene	50	+4%	+0%	+2%	+2%	+6%
MACR	178	−35%	−37%	−37%	-	−37%
MVK	150	−87%	−87%	−86%	−91%	−91%

[a]By Apel-Riemer Environmental Inc., U.S.
[b]By Institute of Arctic and Alpine Research (INSTAAR), University of Colorado, Boulder, U.S.

a high-sensitivity proton transfer reaction mass spectrometer (PTR-MS, Ionicon Analytic GmbH, Austria; manufactured March 2008) between July 2009 and August 2012 at the KCMP tall tower. The PTR-MS was operated at ~130–140 Td under a drift tube pressure of 2.1–2.3 mbar (drift tube voltage 600 V, reaction chamber temperature 60°C, and extraction voltages 50 V; details in Table S1). VOC measurements were made every ~3 min with dwell times ranging from 5 to 20 s for the various chemical species (10 s for *m/z* 69 and *m/z* 71; Table S2). Ambient air was sampled via perfluoroalkoxy (PFA) tubing at 185 m above ground level, thus providing a highly temporally resolved signal that is more regionally representative than obtainable with measurement near the surface [*Hu et al*., 2011, 2013; *Kim et al*., 2013].

The sampling line was kept at ambient temperature, except the final ~1 m which was maintained at 60°C. Ambient air was sampled at ~12 standard l m^{-1}, leading to a residence time in the inlet system of approximately 2 min under normal sampling conditions. A series of experiments in our laboratory showed no detectable VOC wall loss or interference associated with the >185 m PFA inlet line for compounds reported here [*Hu et al*., 2011; see also *Schnitzhofer et al*., 2009]. The PTR-MS was maintained in an air-conditioned building at the base of the tower. It was automatically calibrated in situ every 23 h or every 47 h (before or after August 2010, respectively) via six different standard additions each separated by ~2–5 h. Calibration took place in the final ~2 m of the inlet system by dynamic dilution of multicomponent standards (Apel-Riemer Environmental Inc., U.S.) into zero air generated by passing ambient air through a heated platinum bead catalyst (450°C; Shimadzu Corp., Japan). Instrument background levels were checked every ~2–5 h before and after each calibration for ~15–30 min (5–10 measurement cycles) by measuring zero air as described above. The ambient data were then calibrated based on linear interpolation of the adjacent calibration and background measurements; day-to-day variability of the calibration response was <10% for all species measured at the KCMP tall tower (Table S2). A schematic of the sampling setup is shown in the supporting information (Figure S1), and a more detailed description of the PTR-MS calibration and sampling system is provided by *Hu et al*. [2011].

In parallel with the PTR-MS measurements, a series of air samples were collected on solid adsorbent cartridges to test both the specificity of the PTR-MS measurements and the stability of the VOC standards used for PTR-MS calibration [*Hu et al*., 2013]. A total of 100 ambient samples (plus 25 calibration gas samples for standard intercomparison) were collected using a custom-built autosampler [*Helmig et al*., 2004] between December 2010 and August 2012. All cartridge samples were subsequently analyzed by thermal desorption with gas chromatography and mass selective and flame ionization detectors (GC-MS/FID) at the Institute of Arctic and Alpine Research (INSTAAR), University of Colorado, Boulder, U.S. A detailed description of the cartridge sampling and quantification system used in this work is provided by *Hu et al*. [2013] and *Helmig et al*. [2004].

The premixed VOC standard cylinders used for PTR-MS calibration were originally filled in December 2008 to nominal mixing ratios of 50 ppbv for isoprene, 150 ppbv for MVK, and 178 ppbv for MACR. The cylinders were recertified in January 2012, at which time isoprene was nearly unchanged at 53 ppbv, but MVK and MACR had decreased by 90% and 35%, respectively (to 14 ppbv for MVK and 112 ppbv for MACR). These results were confirmed by cartridge samples collected from December 2010 through July 2011. Cartridge measurements of our calibration standards over this time period indicate that relative to the INSTAAR VOC standards: (i) the isoprene mixing ratio was stable and consistent with the original certification (51 ppbv as measured by cartridge + GC-MS/FID); (ii) the MACR mixing ratio was stable but 37% lower than the original certification (and consistent with the January 2012 recertification); (iii) the MVK mixing ratio was 85%–90% lower than the original certification (Table 1). We thus restrict the present analysis to the time period from January 2011 to December 2011. Calibrations for MVK + MACR are based on the recertified MACR standard (112 ppbv) and follow the

approach of *de Gouw et al.* [2003] to calculate a weighted instrument response factor for the sum of MVK and MACR based on the measured MACR sensitivity and its typical sensitivity and abundance relative to MVK [*Stroud et al.*, 2001; *de Gouw et al.*, 2003; *Baasandorj et al.*, 2015]. The resulting detection limits (at 10 s dwell time) are 38 pptv for isoprene and 21 pptv for MVK + MACR (see Table S2). Estimated uncertainties for the hourly isoprene and MVK + MACR measurements used in this study are ≤15% on average; standard errors associated with the 1 h averaging windows make the largest contribution to this (~2/3), followed by the various sources of instrumental error (e.g., mass flow measurement, calibration factors, and fit). All VOC data presented here, along with concurrent measurements of other VOCs and CO from the KCMP tall tower, are publicly available at www.atmoschem.umn.edu/data.htm.

2.3. GEOS-Chem Chemical Transport Model

We use a nested grid version of the GEOS-Chem CTM (version 9-01-03) to simulate isoprene and MVK + MACR mixing ratios at the KCMP tower. The model is driven by GEOS-5.2 assimilated meteorological data from the NASA Goddard Modeling and Assimilation Office, with 0.5° × 0.667° horizontal resolution over North America (10°–70°N and 140°–40°W), 47 vertical layers extending from Earth's surface to 0.01 hPa, and time steps of 10 min (transport and convection) and 20 min (emissions and chemistry) [*Bey et al.*, 2001]. A global 4° × 5° simulation is used to generate the lateral boundary conditions (for all species, at each vertical layer, every 3 h) required for the nested grid runs [*Wang et al.*, 2004; *Chen et al.*, 2009; *Zhang et al.*, 2011; *van Donkelaar et al.*, 2012]. A 1 year spin-up for 2010 is used to initialize the simulation for 2011, the period of this study. A detailed description of the GEOS-Chem CTM can be found at www.geos-chem.org.

In particular, for this work we use the Emissions Database for Global Atmospheric Research (EDGAR) monthly inventory for global CO, NO_x, and SO_2 emissions [*Olivier and Berdowski*, 2001]. Global anthropogenic VOC emissions are from the Reanalysis of the Tropospheric Chemical Composition (RETRO) inventory [*Schultz et al.*, 2007], which is implemented in GEOS-Chem as described by *Hu et al.* [2015]. Anthropogenic emissions (CO, NO_x, SO_x, NH_3, and VOCs) over the U.S. are taken from the Environmental Protection Agency's (EPA's) National Emission Inventory for 2005 (NEI05; http://www.epa.gov/ttnchie1/net/2005inventory.html) and scaled to the simulation year. In particular, this results in NO_x emissions of 4.5 TgN in the contiguous U.S. during 2011, 30% lower than in 2005 [e.g., *Russell et al.*, 2012]. Biomass burning emissions are computed based on the monthly Global Fire Emission Database version 3 inventory [*van der Werf et al.*, 2010] and measured species: species open fire emission ratios [*Andreae and Merlet*, 2001]. The above emission inventories (as implemented in GEOS-Chem) do not include any anthropogenic sources of isoprene or MVK + MACR.

For this work, we implement the latest version of the Model of Emissions of Gases and Aerosols from Nature (MEGANv2.1) [*Guenther et al.*, 2012] within GEOS-Chem to calculate biogenic emissions of isoprene and other VOCs. MEGANv2.1 computes emissions for each model grid cell based on the fractional coverage of 15 plant functional types and their corresponding base emission factors for VOCs under standard conditions (air temperature = 303 K, photosynthetic active radiation (PAR) = 1500 μmol m^{-2} s^{-1}, and leaf area index (LAI) = 5). Deviations from these standard conditions are accounted for using a set of nondimensional activity factors [*Guenther et al.*, 2012]. PAR (diffuse and direct) and 2 m air temperature from the GEOS-5.2 assimilation system, and monthly mean LAI derived from Moderate Resolution Imaging Spectroradiometer (MODIS) observations [*Myneni et al.*, 2007] (LAI of year 2008 for all ensuing years) are employed to calculate the activity factors for solar radiation, temperature, LAI, and leaf age (γ_{PAR}, γ_T, γ_{LAI}, and γ_{age}). Compounds undergoing bidirectional exchange (formaldehyde, acetaldehyde, ethanol, formic acid, and acetic acid) are treated as described by *Millet et al.* [2010] and *Guenther et al.* [2012]. The resulting isoprene flux for the U.S. domain (25°–50°N; 130°–65°W) is 12.5 TgC for summer 2011 (Figure 1). We do not include here any soil moisture effect on isoprene emissions, a factor that could decrease the global flux by 20% but which is not expected to be important in the region of this study [*Müller et al.*, 2008].

Later, we compare the model γ_T values to those calculated with the surface air temperature observed (3 m above ground level) at the KCMP tall tower to quantify the extent to which errors in the GEOS-5.2 assimilated air temperature fields bias the simulated isoprene (and MVK + MACR) mixing ratios. The temperature activity factor for isoprene is calculated according to the MEGANv2.1 algorithms:

$$\gamma_T = E_{\text{opt}} \left[200 \frac{\exp(C_{T1}\, x)}{200 - C_{T1}\,(1 - \exp(200\, x))} \right], \tag{1a}$$

Table 2. Fractional Coverage of Plant Functional Types (PFTs) for the GEOS-Chem Model Grid Cell Containing the KCMP Tall Tower, According to the CLM4 and USDA-NASS Land Cover Data Sets[a]

	Barren (%)	Crop (%)	Developed (%)	Deciduous (%)	Evergreen (%)	Shrub (%)	Grass (%)	Sum (%)	Total EF[b] (μg/m^2/h)
EF (μg/m^2/h)	0	1	0	10000	600	4000	800	-	-
USDA-NASS	0.18	50.5	15.5	12.2	0.04	1.0	20.6	100	1425
CLM4	0.03	58.8	-	5.1	0.64	-	31.3	95.9	769

[a]Also shown is the isoprene base emission factor (EF) for each PFT according to MEGANv2.1.
[b]Total EF: weighted total emission factor across all PFTs, calculated as the sum of products of the fractional coverage for each PFT and the corresponding emission factor.

where

$$x = \frac{\left[\left(\frac{1}{T_{\text{opt}}}\right) - \frac{1}{T}\right]}{0.00831} \tag{1b}$$

$$T_{\text{opt}} = 313 + (0.6\,(T_{240} - 297)) \tag{1c}$$

$$E_{\text{opt}} = C_{eo} \times \exp(0.08\,(T_{240} - 297)). \tag{1d}$$

In equations (1a)–(1d), T is the 2 m air temperature, which is assumed equivalent to the leaf temperature over forests [*Palmer et al.*, 2003; *Guenther et al.*, 2006; *Millet et al.*, 2008], and T_{240} is the average surface air temperature over the past 240 h. C_{T1} and C_{eo} are both VOC-dependent empirical coefficients, equal to 95 and 2, respectively, in the case of isoprene.

Our implementation of MEGANv2.1 within GEOS-Chem uses the Parameterized Canopy Environment Emission Activity (PCEEA) algorithm described in *Guenther et al.* [2006] and (as a default) PFT distributions from version 4 of the Community Land Model (CLM4; native spatial resolution 0.47° × 0.63°) [*Oleson et al.*, 2010]. For the present work, we also use a second land cover database for the region surrounding the KCMP tall tower, from the 2007 U.S. Department of Agriculture National Agricultural Statistics Service (USDA-NASS) Cropland Data layer product (native spatial resolution of 30 m × 30 m for 2011; http://www.nass.usda.gov/research/Cropland/SARS1a.htm). Land cover differences between CLM4 and USDA-NASS are substantial over this transitional region between high-isoprene emitters (broadleaf trees with base emissions of 10^4 μg m^{-2} h^{-1}) and nonemitters (crops with base emissions of 10^0 μg m^{-2} h^{-1}) (Figure 2 and Table 2). For example, broadleaf tree coverage within the model grid cell containing our tall tower is 12.2% according to the USDA-NASS data set but only 5.1% according to CLM4. This leads to a twofold difference in the derived annual emission factor for isoprene in the two cases (1430 μg m^{-2} h^{-1} for USDA-NASS versus 770 μg m^{-2} h^{-1} for CLM4; Table 2). Later, we will assess how these differences affect the interpretation of our results.

The GEOS-Chem chemical mechanism includes detailed HO_x-NO_x-VOC-ozone chemistry coupled to aerosols, employing the most recent Jet Propulsion Laboratory and International Union of Pure and Applied Chemistry recommendations as described by *Mao et al.* [2010]. The isoprene oxidation scheme used here follows *Paulot et al.* [2009a, 2009b] for high-NO_x and low-NO_x conditions, respectively. Dry deposition is computed using a resistance-in-series model [*Wesely*, 1989], with reactive uptake for oxygenated VOCs prescribed according to *Karl et al.* [2010].

Later, an ensemble of sensitivity simulations with varying model assumptions for emissions, chemistry, atmospheric mixing, dry deposition, and land cover is performed to test the robustness of our results; see Table S3 in the supporting information.

3. Specificity of PTR-MS Measurements for Isoprene (*m/z* 69) and MVK + MACR (*m/z* 71)

Several previous studies have pointed out that isoprene measurements by quadrupole PTR-MS at *m/z* 69 can be subject to interferences from (i) other biogenic VOCs such as 2-methyl-3-buten-2-ol (232-MBO) [*de Gouw and Warneke*, 2007; *Karl et al.*, 2012], (ii) furan in biomass burning plumes [*Christian et al.*, 2004], (iii) a variety of alkenes and cycloalkanes in urban air and oil/gas extraction areas [*de Gouw et al.*, 2003; *Yuan et al.*, 2014; *Warneke et al.*, 2014], and (iv) C5 compounds such as pentenols and methylbutanal emitted via plant wounding during harvesting [*Karl et al.*, 2001]. There is also known to be a small anthropogenic source of isoprene and MVK + MACR associated with tailpipe emissions [*McLaren et al.*, 1996; *Borbon et al.*, 2001; *Park et al.*, 2011; *von Schneidemesser et al.*, 2011; *Wang et al.*, 2013; *Wagner and Kuttler*, 2014].

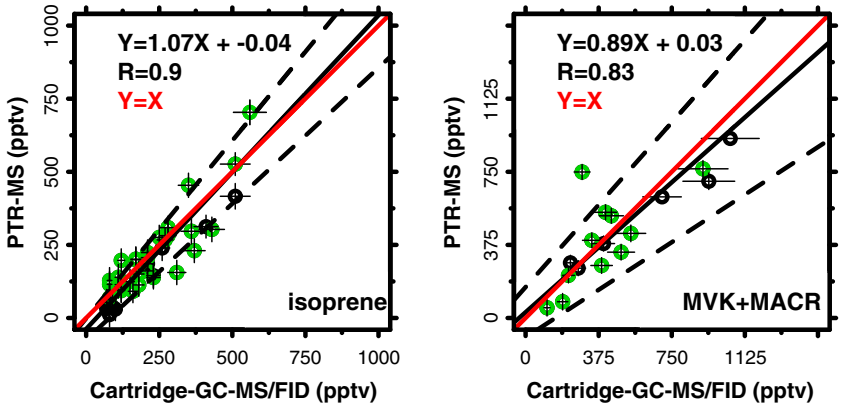

Figure 3. Intercomparison between PTR-MS and cartridge-GC-MS/FID measurements at the KCMP tall tower. (left) PTR-MS measurements at *m/z* 69 versus isoprene as measured by cartridge-GC-MS/FID (December 2010 to August 2012). (right) PTR-MS measurements at *m/z* 71 versus MVK + MACR as measured by cartridge-GC-MS/FID (July–August 2012). Data points are colored to indicate daytime (green dots) versus nighttime (black dots) measurements. Black solid lines show the best fit from a major axis regression, with parameters given inset. Dashed lines show the 95% confidence interval for the best fit. The 1:1 line is shown in red. Error bars indicate the 95% confidence interval for each measurement.

We employ here two independent approaches to quantify the contribution of the above interferences (and any anthropogenic isoprene sources) to the tall tower isoprene and MVK + MACR measurements. First, ambient PTR-MS observations are compared with concurrent speciated measurements by cartridge-GC-MS/FID. Figure 3 shows that the two measurements agree to within their combined uncertainties (~25%), for both isoprene and MVK + MACR, and for both daytime and nighttime measurements. This argues against any significant role for the interferences i–iv above. Furthermore, C5 compounds associated with plant wounding should be most important during harvesting, which typically takes place in mid-October or later in this region [*Chen et al*., 2015], outside of our main period of analysis (June–August).

In the second approach, we use the source tracer technique described by *Hu et al*. [2011], which had an estimated uncertainty of ±30% when applied to methanol. Here we use C_8 and C_9 aromatic VOCs as anthropogenic tracers, since their atmospheric lifetimes are comparable to those of isoprene and MVK + MACR (i.e., on the order of hours). We employ wintertime (December–February) measurements to derive anthropogenic enhancement ratios for isoprene and MVK + MACR relative to C_8 aromatics and C_9 aromatics (Table 3), under the assumption that biogenic influences at this time are negligible. We then assume that the same enhancement ratios can be employed year round to quantify the nonbiogenic signal at *m/z* 69 and *m/z* 71. Figure 4 shows the resulting year-round anthropogenic contributions to the measured *m/z* 69 and *m/z* 71 signals at the KCMP tall tower, as well as their summertime diurnal cycles. Applying either C_8 or C_9 aromatics as the anthropogenic tracer yields results that in general agree to within 10%.

Based on this approach, we find that the nonbiogenic contribution to the *m/z* 69 signal measured at the KCMP tall tower averages 22% (95% confidence interval: 18%–26%) during summer daytime (June–August, 10:00–17:00 CST) and 31% over the whole summer (Figure 4). It contributes up to 80% of the observed *m/z* 69 signal during the night and early morning, when anthropogenic emissions can accumulate in the shallow boundary layer. The absolute anthropogenic contribution is consistently between 30 and 46 pptv, close to the PTR-MS detection limit for isoprene (38 pptv). The anthropogenic contribution to the *m/z* 71 signal abundance is smaller (19–26 pptv), amounting to only 7% of the total during summer daytime and 8% over the whole summer (Figure 4).

Table 3. Correlation[a] Between C_6 – C_9 Aromatics and Observed Signals at *m/z* 69 and *m/z* 71 During Winter (December–February)

	Benzene			Toluene			C_8 aromatics			C_9 aromatics			
	Slope	Intercept	*R*	Slope	Intercept	*R*	Slope	Intercept	*R*	Slope	Intercept	*R*	*N*
m/z 69	0.70	−0.08	0.72	0.51	0	0.81	0.33	0.01	0.82	0.89	0	0.79	1590
m/z 71	0.47	−0.04	0.62	0.34	0	0.68	0.22	0	0.69	0.59	0	0.67	1590

[a] *m/z* 69 (or *m/z* 71) = aromatic species × slope + intercept.

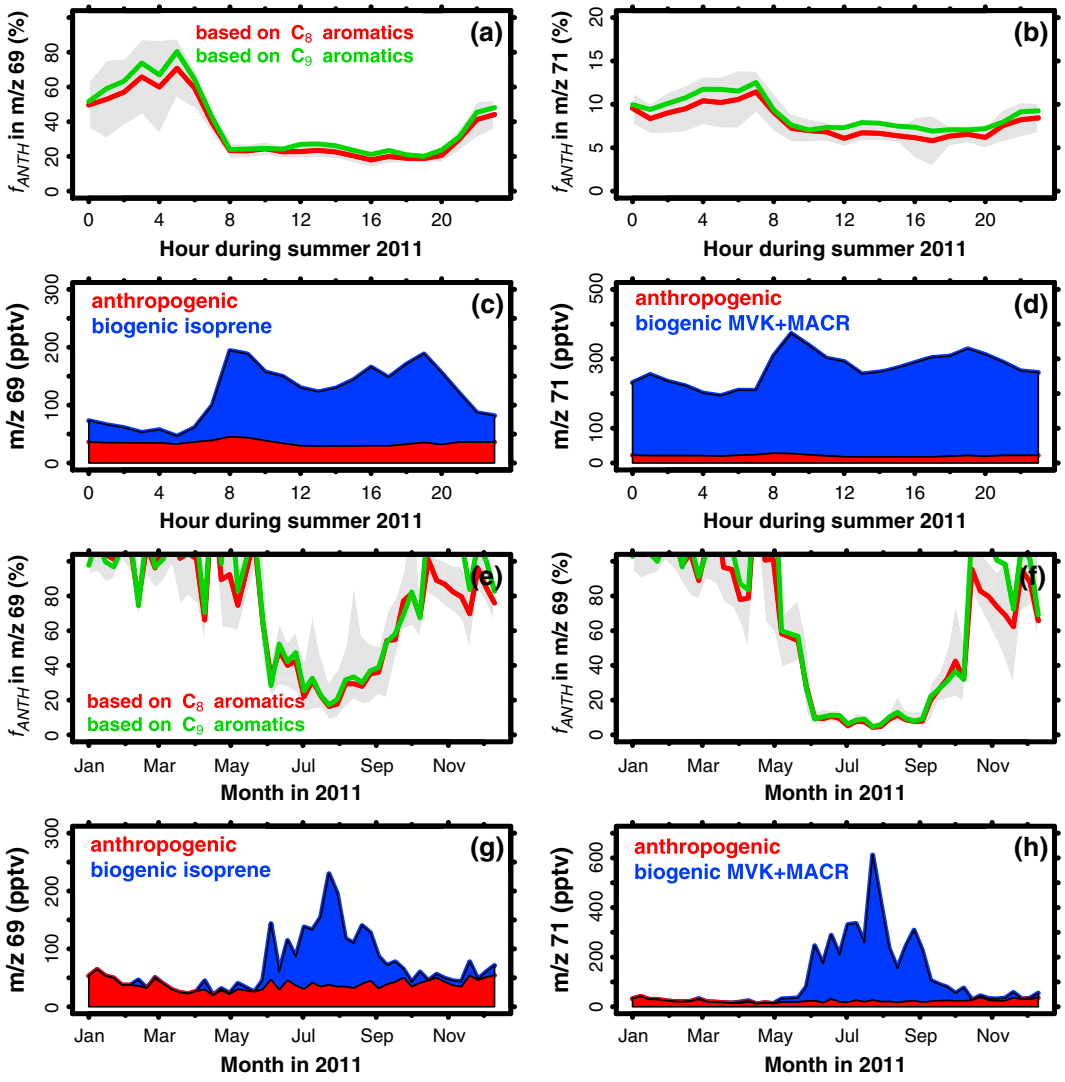

Figure 4. Anthropogenic and biogenic contributions to the *m/z* 69 and *m/z* 71 signals measured by PTR-MS at the KCMP tall tower during 2011. (first row) Diurnal fractional contribution (hourly median) of anthropogenic sources (f_{ANTH}) to the *m/z* 69 and *m/z* 71 signals during summer 2011 (June–August), estimated using different anthropogenic tracers (blue: C_8 aromatics; red: C_9 aromatics). Shaded areas represent the 95% confidence interval of the estimates based on C_8 aromatics. (second row) Stack plots of the diurnal biogenic and anthropogenic contributions to the *m/z* 69 and *m/z* 71 signals during summer 2011, estimated using C_8 aromatics as the anthropogenic tracer (hourly median). (third and fourth rows) Same as the first and second rows, except showing the seasonal anthropogenic and biogenic contributions (based on weekly medians).

The comparisons between the PTR-MS and the cartridge-GC-MS/FID measurements of isoprene and MVK + MACR in Figure 3 do not show any evidence of a high bias for the PTR-MS, even during nighttime. This suggests that the nonbiogenic component inferred above may be predominantly due to anthropogenic isoprene (and MVK + MACR) as opposed to interfering isobaric compounds.

In the following sections, we subtract the anthropogenic contributions from the observed *m/z* 69 and *m/z* 71 signals, and treat the residuals as biogenic isoprene and MVK + MACR, respectively. These can then be compared directly with the corresponding quantities simulated by GEOS-Chem, which include only biogenic contributions. We note that the model-measurement comparisons discussed below focus on daytime during summer, when the role of anthropogenic interferences is modest in any case.

Some recent work indicates that isoprene hydroxyhydroperoxides (ISOPOOH) and possibly isoprene epoxydiols (IEPOX) can be detected along with MVK + MACR at *m/z* 71, which would complicate the interpretation of measurements at this mass [*Liu et al.*, 2013; *Rivera-Rios et al.*, 2014]. Since GC-based measurements can also be

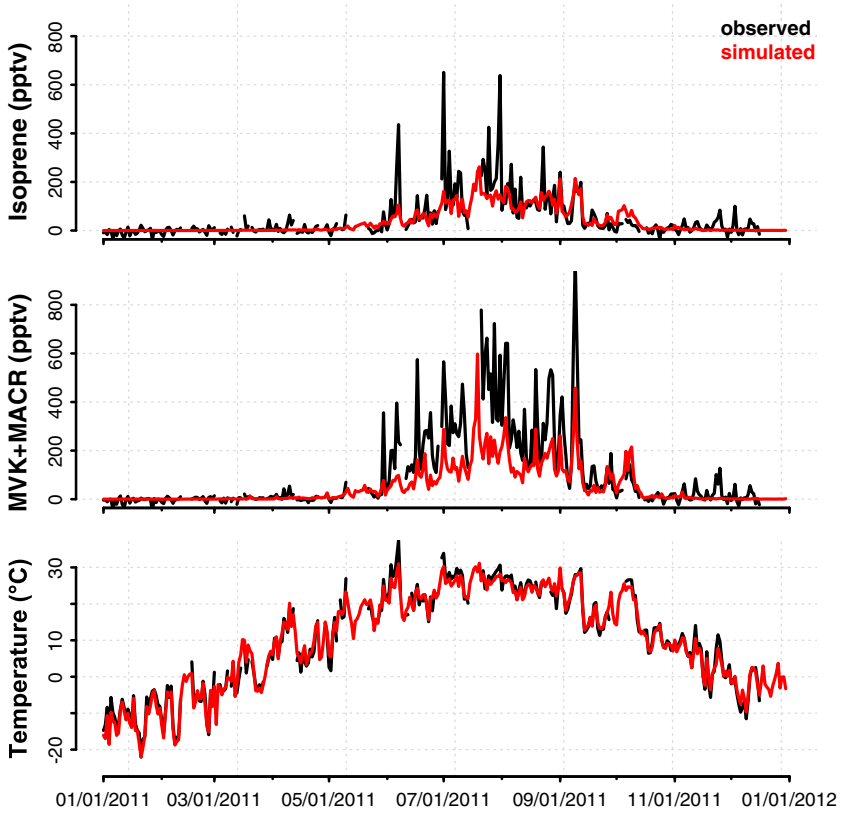

Figure 5. Annual cycle of biogenic isoprene and MVK + MACR mixing ratios and surface air temperature (3 m) measured at the KCMP tall tower in 2011 (black; daytime averages for 10:00–17:00 CST). Anthropogenic contributions to the *m/z* 69 and *m/z* 71 signals have been removed as described in the text. Also shown are the isoprene and MVK + MACR mixing ratios simulated by GEOS-Chem (using CLM4 vegetation; the inverse distance-weighted mean from the four intersecting grid cells as described in the text), and the assimilated surface air temperatures (2 m) used to drive the model (red).

subject to the same interference, the PTR-MS versus cartridge-GC-MS/FID comparisons discussed above do not necessarily provide a robust test for this specific issue. However, given the significant observed NO_x levels in the area (section 6) and the generally small ratio of isoprene hydroxyhydroperoxides to MVK + MACR in GEOS-Chem for the region of our study (summer daytime average 0.06), we do not expect a major contribution from such species. In section 5, we perform a dedicated model sensitivity test to explore the potential impact of this assumption.

4. Isoprene and Its Oxidation Products in the U.S. Upper Midwest

Figure 5 shows daytime average (10:00–17:00 CST) isoprene and MVK + MACR mixing ratios measured at the KCMP tall tower during 2011, along with the measured surface air temperatures (CSAT3, Campbell Scientific Inc., USA) and the assimilated temperatures used to drive GEOS-Chem and MEGAN. Figure 6 plots the daytime average mixing ratios of isoprene and MVK + MACR, the isoprene/(MVK + MACR) ratio, and γ_T (equations (1a)–(1d)) calculated based on the measured and assimilated surface air temperatures, for the growing season only.

Pronounced seasonal cycles are seen for isoprene and MVK + MACR, with elevated mixing ratios during the May–September growing season reaching maxima (for 1 h mean) of 2540 pptv (isoprene) and 2790 pptv (MVK + MACR). Onset of isoprene emissions began around 30 May (day of year 151) in the vicinity of the KCMP tall tower, when the average daytime air temperature reached 27°C; for the most part daytime temperature then remained above 20°C throughout the ensuing summer. The observed mixing ratios of isoprene and its oxidation products then decreased rapidly in mid-September once daytime temperatures dropped below 20°C (at which point γ_T dropped to almost zero; Figure 6). This timing of the annual cycle is consistent with that observed at Harvard Forest (which is at a similar latitude as the KCMP tall tower), reflecting the concurrent drivers of plant phenology and associated temperature changes on the seasonal course of isoprene emissions [*Goldstein et al.*, 1998].

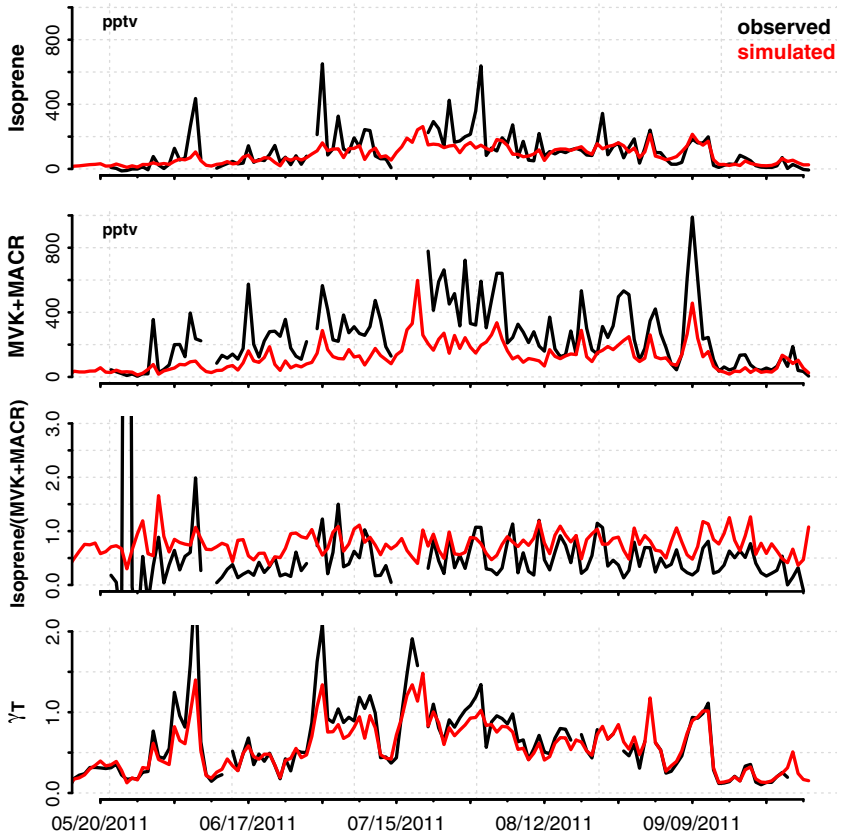

Figure 6. Daytime (10:00–17:00 CST) average isoprene, MVK + MACR, isoprene/(MVK + MACR), and γ_T values computed based on the surface air temperature at the KCMP tall tower during the growing season (20 May 2011 to 31 September 2011). Measurements (in black) are compared to the corresponding simulated values from GEOS-Chem using CLM4 land cover (in red). Anthropogenic contributions to the measured isoprene and MVK + MACR mixing ratios have been removed as described in the text.

Figure 7 shows the average summertime diurnal cycles for isoprene, MVK + MACR, the isoprene/(MVK + MACR) ratio, C_8 aromatics, and surface air temperature as a function of wind direction at the KCMP tall tower. A notable feature in these polar annulus plots is that elevated isoprene and MVK + MACR mixing ratios are frequently observed at night with winds from the northeast and east. Mixing ratios for anthropogenic tracers such as the C_8 aromatics are also enhanced at night in the shallow nocturnal boundary layer (Figure 7), but these exhibit a different diurnal cycle tied to morning and evening rush hours, and are most strongly associated with a distinct wind direction (i.e., winds from the north transporting pollution from the Twin Cities). The fact that the nighttime enhancements of MVK + MACR originate from a wider swath of wind direction and persist for longer periods of time than those of isoprene implies that they arise from biogenic sources somewhat distant from the tall tower. This is consistent with the extensive broadleaf tree cover to the north and east of the KCMP tall tower (Figure 2). Such transport of isoprene and its oxidation products into the Twin Cities area at night will likely drive nighttime chemistry involving NO_3 and O_3 as well as the formation of gas- and aerosol-phase nitrates [*Brown et al.*, 2013].

We see in Figure 7 that elevated temperatures and daytime isoprene enhancements tend to be associated with winds from the southwest, indicating nearby emissions in this direction. Under these conditions, the isoprene/(MVK + MACR) ratio is relatively high ($\geq$1), indicating an approximate transport time less than one isoprene lifetime (e.g., $<$ 27 km with a mean wind speed of 5 m/s and an 82 min isoprene lifetime). On the other hand, the mean isoprene/(MVK + MACR) ratio from other wind directions (i.e., excluding 170°–280°) is only 0.30 (Figure 6 and Figure 8 (left)), indicating more regional aged emissions with aggregate effective transport of ~50 km (under the same assumptions as above).

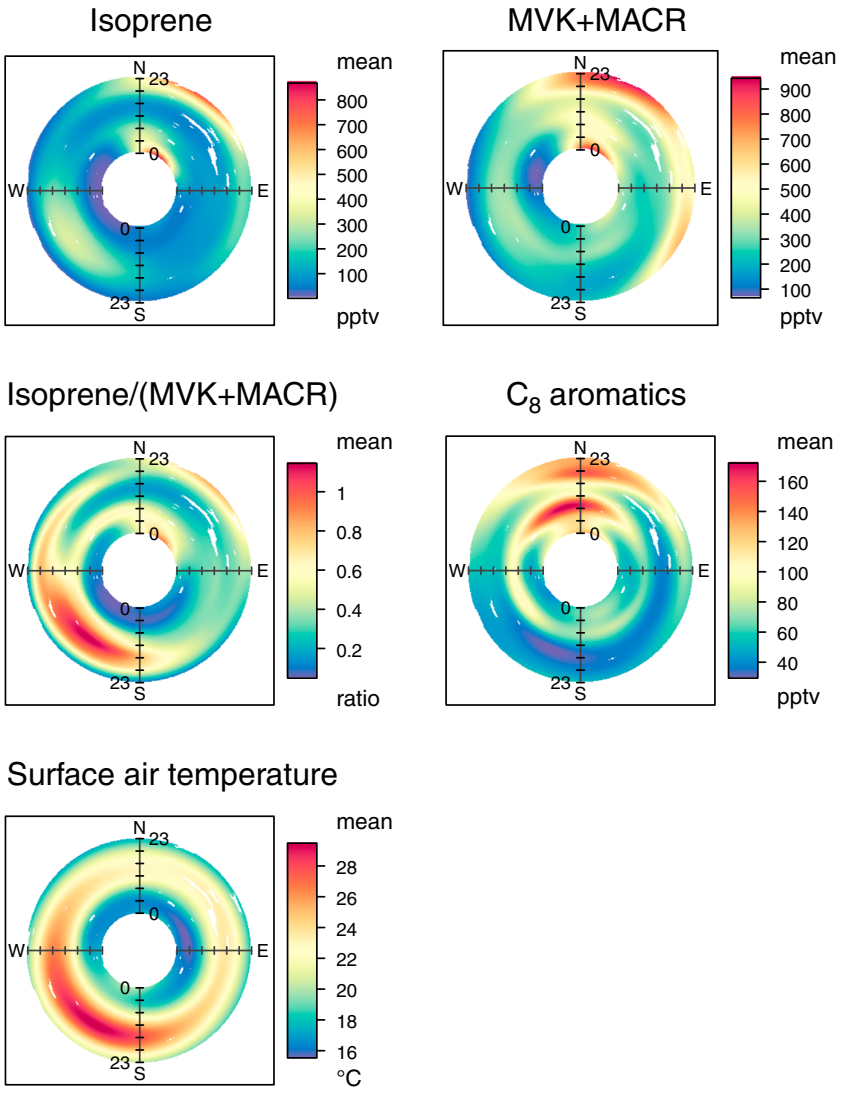

Figure 7. Diurnal cycle as a function of wind direction for isoprene, MVK + MACR, the isoprene/(MVK + MACR) ratio, C_8 aromatics, and surface air temperature as measured during summer 2011 at the KCMP tall tower. Plots were generated using the open source R package openair [*Carslaw and Ropkins*, 2012].

5. Model Underprediction of Regional Isoprene Emissions

Initial model:observation comparisons revealed a dramatic low model bias when using CLM4 land cover to drive biogenic emissions in MEGANv2.1: a factor of 6.0 for isoprene and 5.4 for MVK + MACR during daytime (10:00–17:00 CST) in summer 2011. When using the higher-resolution USDA-NASS land cover, these model biases were reduced by one half to one third (to factors of 2.7 and 3.5, respectively). The simulated isoprene emissions are thus extremely sensitive to the selection of land cover for this region: in this transitional landscape with ~5–15% broadleaf tree cover, a small absolute error in the estimated PFT fractions can lead to a large discrepancy in the simulated isoprene emissions and abundance (Figure 2 and Table 2).

In addition, Figure 2 shows that the KCMP tall tower is located near the intersection of four GEOS-Chem grid cells, with the adjoining three cells having more than twice the broadleaf tree coverage of the cell containing the tower (>11% versus 5%) according to CLM4. This type of representation error is dependent on the model resolution and is a particular issue for short-lived tracers such as isoprene and MVK + MACR. To minimize its effect here, we use inverse distance-weighted model mixing ratios for the model:observation comparisons below. Specifically (and unless indicated otherwise), the simulated mixing ratios at the tall tower

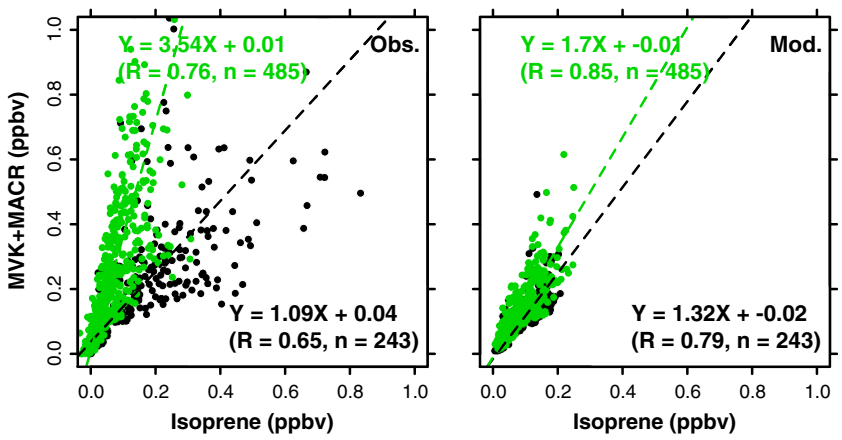

Figure 8. Correlation between MVK + MACR and isoprene mixing ratios during summer daytime (10:00–17:00 CST) as (left) measured at the KCMP tall tower and (right) simulated by GEOS-Chem using CLM4 land cover. Data are colored according to wind direction: black dots indicate southwesterly winds (170°–280°) and green dots indicate all other wind directions. Dashed lines show the major axis regression best fit lines for the corresponding data subsets, with parameters given inset.

are taken as the mean from the four intersecting grid cells, with each value weighted by the inverse distance between the center of that grid cell and the tall tower. The average low biases in the base model for summer daytime are then reduced to factors of 2.4 (1.8 when using NASS) for isoprene and 2.6 (2.3 when using NASS) for MVK + MACR relative to the KCMP tall tower observations.

Figure 5 shows the resulting simulated isoprene and MVK + MACR mixing ratios in the base-case simulation using CLM4 vegetation (red; daily 10:00–17:00 CST averages), along with the assimilated surface air temperature that is used to compute the BVOC fluxes within MEGANv2.1. We see that the base model captures the seasonal cycle for isoprene and its oxidation products, including the timing of the onset and shutdown of isoprene fluxes in the spring and fall. For most of the growing season, there is little bias in the modeled isoprene mixing ratios (Figure 6). However, the model cannot reproduce the periodic large enhancements seen in the observations; the low model bias during these events is associated with a corresponding low bias in the GEOS-5.2 temperatures (and therefore γ_T; equations (1a)–(1d)) that manifests during these same periods (Figure 6). On the other hand, the low bias in the simulated MVK + MACR mixing ratios shows little to no correlation with γ_T (Figure 5).

We next compare the hourly simulated and observed isoprene and MVK + MACR mixing ratios as a function of wind direction (Figure 9). When the wind is not out of the southwest (wind directions other than 170°–280°), the simulated isoprene mixing ratios show only a small bias compared to the observations (−18%; 95% confidence interval (CI): −10% to −26%), which can be explained by a comparable bias in the GEOS-5.2 temperatures used in GEOS-Chem: the simulated γ_T values are 18% (95% CI: 15%–22%) too low based on the observed surface temperatures at the KCMP tall tower. On the other hand, when the wind is out of the southwest (170°–280°; black), the simulated isoprene mixing ratios show a significant low bias compared to the observations (−70%; 95% CI: −64% to −73%). The low bias in the assimilated temperatures (−40% in γ_T under these conditions; 95% CI: −35% to −45%) is a main driver of this discrepancy (Figure 9). In addition, as discussed in section 4, there is clearly a distinct source region to the southwest of our tall tower that is within one isoprene *e*-folding distance (and therefore also within one model grid cell). This type of near-field effect cannot be captured at the ~50 km × 50 km resolution of our simulation (Figure 8).

Model:observation comparisons for MVK + MACR are more stable than for isoprene and do not vary significantly with wind direction: on average, the simulated MVK + MACR mixing ratios are 61% (95% CI: 56%–67%) lower than the KCMP tall tower observations. Next, we test the robustness of the above comparisons to a variety of model assumptions, and assess what conclusions can be drawn regarding the emissions and impacts of isoprene in this region.

To this end, we repeat the above model:observation comparisons while varying key model parameters to test the robustness of the overall results. These tests include a number of differing assumptions for model chemistry: (i) including versus excluding bromine chemistry, which modifies the model oxidant fields [*Parrella*

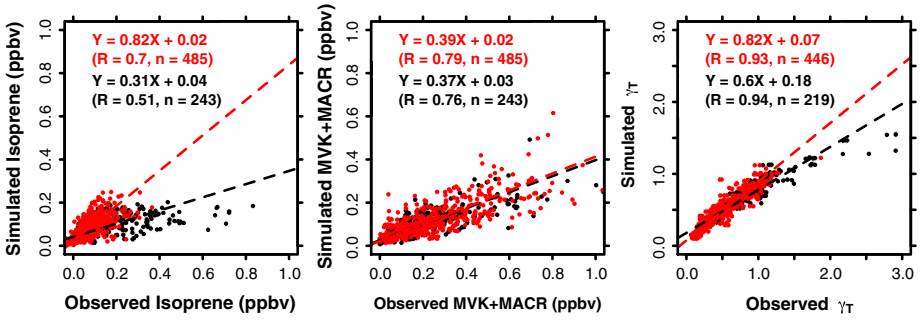

Figure 9. Model:measurement comparisons at the KCMP tall tower during summer daytime (10:00–17:00 CST). Measured mixing ratios of isoprene and MVK + MACR, and γ_T values computed based on the observed surface air temperatures, are compared to the simulated values from GEOS-Chem using CLM4 land cover. Data are colored by wind direction, with black dots indicating southwesterly winds (170°–280°) and red dots indicating all other wind directions. Dashed lines show the major axis regression best fits for the corresponding data subsets, with parameters given inset.

et al., 2012]; (ii) varying the reactive uptake coefficient for HO_2 on aqueous aerosol [*Mao et al*., 2013]; (iii) employing an updated (and more rapid) rate of reaction ($k = 2.91E\text{-}13 \times EXP(1300/T)[1\text{-}EXP(-0.245n)]$; n = # of carbon atoms) for >C2 RO_2 radicals with HO_2 compared to the base case ($k = 7.40E\text{-}13 \times EXP(700/T)$); (iv) employing the previous model representation of isoprene chemistry [*Palmer et al*., 2006; *Millet et al*., 2008]; and (v) altered NO_x emissions. The latter include runs with NO_x emissions reduced by 10% and 50%, as well as a run in which the NO_x emissions in the vicinity of the tower are spatially redistributed (see Table S3). We also perform sensitivity runs with differing treatment of (vi) dry deposition (using a coefficient for reactive uptake of MVK and MACR by vegetation of 0 rather than 1); (vii) land cover (USDA-NASS versus CLM4); (viii) boundary layer mixing (local versus nonlocal schemes) [*Lin and McElroy*, 2010]; and (ix) isoprene emissions (scaled by values ranging from 0.9 to 1.5). Results are summarized in Figure 10, and a detailed description of all sensitivity runs is given in Table S3. We exclude for this purpose periods with southwesterly winds due to the associated bias in the assimilated surface temperature.

We find that the isoprene bias in the model is not significant when one considers the sensitivity of the simulated mixing ratios to the various model assumptions (Figure 10): model:observation slopes range from 0.42 to 1.53 across different configurations for chemistry, dry deposition, mixing, NO_x emission, and land cover. On the other hand, model biases for MVK + MACR are larger than those for isoprene and are robust across our ensemble of sensitivity runs (Figure 10): the standard model configuration with CLM4 or NASS land cover yields a bias in MVK + MACR of −60%, with a range of −25% to −66% across all the sensitivity tests. Because MVK and MACR are (i) longer lived than isoprene, (ii) produced throughout the atmospheric mixed layer rather than emitted at the surface, and (iii) somewhat chemically buffered (their source as well as their main sink is photochemical), their simulated abundance is much less sensitive to specific model assumptions regarding mixing, dry deposition, chemistry, and fine-scale land cover.

Also included in Figure 10 is a sensitivity run that aims to test how the detection of isoprene hydroxyhydroperoxides as MVK + MACR in the PTR-MS might influence our findings. Here, rather than comparing the measured MVK + MACR with the same quantity from the model, we compare instead the measured MVK + MACR with the modeled sum of MVK + MACR + ISOPOOH + 0.3*IEPOX. The test thus assumes that ISOPOOH is quantitatively converted to MVK + MACR within or upstream of the PTR-MS, while IEPOX is converted with 30% efficiency [*Liu et al*., 2013; *Rivera-Rios et al*., 2014]. This test yields a 15% higher model/observation ratio for MVK + MACR compared to the base case (0.45 versus 0.39 in the base). As with the other sensitivity tests, this is insufficient to resolve the model:observation discrepancy for MVK + MACR. Since the current version of GEOS-Chem does not account for aerosol uptake of IEPOX, which may account for half of its gas phase loss [*Liu et al*., 2015], the derived 15% should be considered a conservative bound on the potential impact of ISOPOOH/IEPOX interferences on our analysis. Another potential uncertainty is the model yield of MVK + MACR, as recent work indicates that the isomeric distribution of isoprene peroxy radicals (and hence the resulting MVK + MACR production) changes as a function of RO_2 lifetime [*Peeters et al*., 2009; *Crounse et al*., 2011]. This could potentially increase the yield of MVK + MACR by a factor of ~1.2 relative to the current version of GEOS-Chem [*Peeters et al*., 2009; *Crounse et al*., 2011]; however, this is again insufficient to resolve the low model bias that we observe.

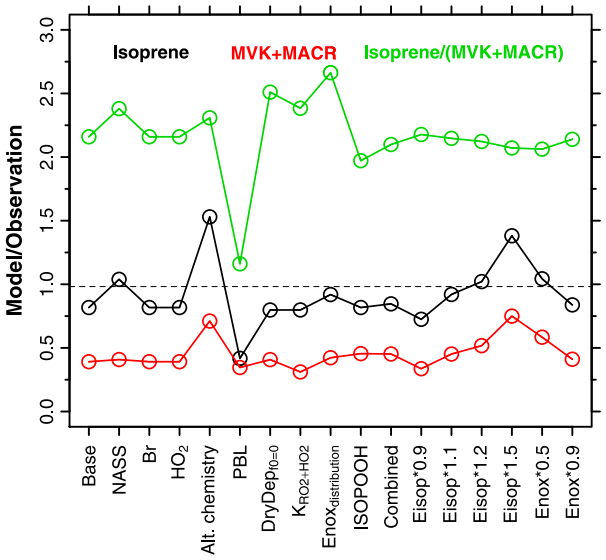

Figure 10. Model/measurement agreement for isoprene (black), MVK + MACR (red), and the isoprene/(MVK + MACR) ratio (green) across an ensemble of sensitivity simulations using GEOS-Chem and MEGANv2.1. Values shown are model:measurement slopes from a major axis regression (in the case of isoprene and MVK + MACR) or the median model:measurement ratio (in the case of isoprene/(MVK + MACR)) for daytime (10:00–17:00 CST) during the 2011 growing season. Periods with southwesterly winds have been excluded (see text). The black dashed line shows the average model/measurement ratio for γ_T computed based on the surface air temperature over the same time interval. *Base*: simulation using CLM4 vegetation, with the model values taken as an inverse distance-weighted mean of the four intersecting grid cells as described in section 5. *NASS*: the same as Base except using USDA-NASS land cover for the region surrounding the KCMP tall tower. *Br*: the same as Base, except including bromine chemistry [*Parrella et al.*, 2012]. *HO_2*: the same as Base, except using a reactive uptake coefficient for HO_2 on aqueous aerosols of 0.4 rather than 0.2 [*Mao et al.*, 2013]. *Alt. chemistry*: previous model representation of isoprene chemistry [*Palmer et al.*, 2006; *Millet et al.*, 2008]. *PBL*: using a local rather than a nonlocal scheme for boundary layer mixing in the model [*Lin and McElroy*, 2010]. *$DryDep_{f0=0}$*: the same as Base, except using a coefficient for reactive uptake of MVK and MACR by vegetation of 0 rather than 1. *$K_{RO2+HO2}$*: the same as Base, except using an updated (and more rapid) rate of reaction for > C2 RO_2 radicals with HO_2. *$Enox_{distribution}$*: the same as Base, except with NO_x emissions in the vicinity of the tall tower redistributed as described in the text. *ISOPOOH*: the same as Base, except the modeled MVK + MACR mixing ratios are adjusted to include potential interferences from ISOPOOH and IEPOX [*Liu et al.*, 2013]. *Combined*: cumulative effect of $DryDep_{f0=0}$, $K_{RO2+HO2}$, $Enox_{distribution}$, and ISOPOOH. *Eisop*x.x*: isoprene emissions multiplied by a factor of x.x. *Enox*x.x*: NO_x emissions multiplied by x.x. See Table S3 in the supporting information for more details.

Taken as a whole, the above findings (persistent low model bias for MVK + MACR but not for isoprene) suggest a general underestimate of isoprene emissions in the broader region but not necessarily in the immediate vicinity of the tower. This is consistent with the fact that the predominant isoprene emitters are concentrated 50 km or more from the tower (Figure 2) and with the aged nature of the biogenic mixture reaching the site (section 4). An alternative explanation for the low model MVK + MACR would be an OH overestimate for this area. Arguing against the latter as the sole explanation is the fact that a sensitivity run with NO_x emissions decreased by 50% did not come close to resolving the discrepancy (Figure 10). This suggests that a major bias in model OH would be required to reconcile the observed and simulated MVK + MACR abundance, and this type of bias is not evident from a previous analysis of benzene: toluene ratios at this site [*Hu et al.*, 2015].

6. Seasonal NO_x-VOC Photochemical Transitions as Controlled by Isoprene Emissions

It is well known that isoprene and other biogenic VOCs play a key role in ozone formation [*Chameides et al.*, 1988; *National Research Council*, 1991; *Jacob et al.*, 1995; *Fiore et al.*, 2005]. Here we use the GEOS-Chem simulation driven by USDA-NASS land cover, which shows reasonable agreement with the KCMP tall tower isoprene observations (though still underestimating MVK + MACR; Figure 10) to examine the role of isoprene emissions in shifting between NO_x- and VOC-limited chemical regimes during the vernal and autumnal seasonal transitions in the U.S. Upper Midwest.

The sensitivity of ozone production to isoprene emissions depends on NO_x [*Fiore et al.*, 2005], which was not measured at the KCMP tall tower. However, we find that the simulated summer daytime NO_2 mixing ratios (computed from the four intersecting grid cells in the same way as for isoprene and MVK + MACR) based on NEI05 emissions are comparable to those measured at a nearby EPA monitoring site (site number 423, ~6 km north of the tall tower; https://ofmext.epa.gov/AQDMRS/aqdmrs.html), particularly when one considers the known tendency of this type of analyzer (chemiluminescence with molybdenum converter) to overestimate NO_2 [*Dunlea et al.*, 2007; *Steinbacher et al.*, 2007; *Lamsal et al.*, 2008; *Boersma et al.*, 2009]: the corresponding NO_2 mixing ratios are 1.5 ± 0.7 ppbv in the model versus 2.2 ± 3.0 ppbv as reported by the EPA (mean ± standard deviation).

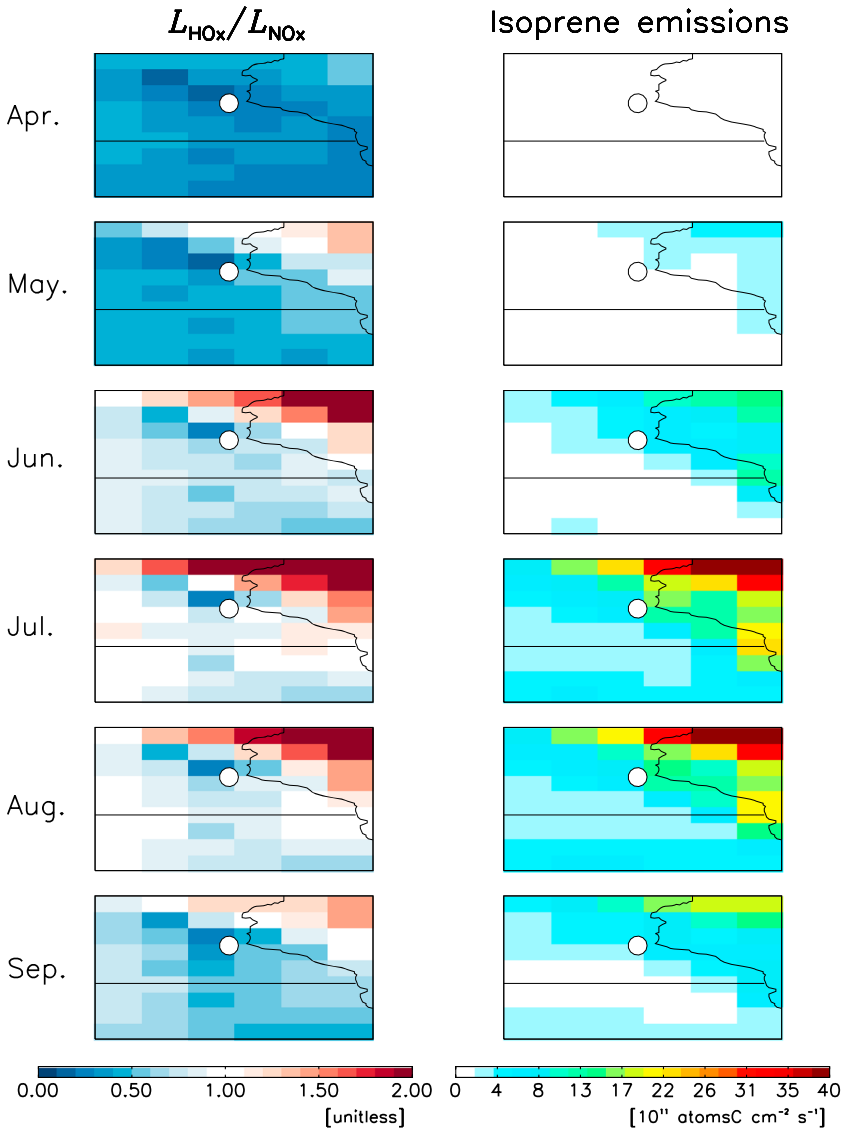

Figure 11. Seasonal evolution of NO_x- versus VOC-limited ozone chemistry in the region surrounding the KCMP tall tower, as simulated by GEOS-Chem. Plotted are the monthly mean daytime (11:00–15:00 CST) L_{HOx}/L_{NOx} ratios and isoprene emissions based on the USDA-NASS land over data set (USDA-NASS, 2007). The white circle indicates the location of the KCMP tall tower. $L_{HOx}/L_{NOx} > 1$: NO_x-limited regime; $L_{HOx}/L_{NOx} < 1$: VOC-limited regime. See text for details.

We use the loss of HO_x radicals via self-reaction (L_{HOx}, where $HO_x = OH + HO_2 + \Sigma RO_2$) relative to the loss of NO_x radicals (L_{NOx}, where $NO_x = NO + NO_2 + NO_3 + HONO$) as an indicator for NO_x- versus VOC-limited O_3 chemistry [*Sillman et al.*, 1990; *Kleinman*, 1994]. The transition between NO_x- and VOC-limited regimes can be defined as the point when $L_{HOx}/L_{NOx} = 1$ [*Duncan et al.*, 2010]. When $L_{HOx}/L_{NOx} > 1$, HO_x radicals tend to react with themselves rather than with NO_x, so that peroxide formation is the main HO_x sink. Under such conditions, production of O_3 is limited by the availability of atmospheric NO_x but is insensitive to moderate changes in VOC abundance (NO_x-limited regime). When $L_{HOx}/L_{NOx} < 1$, loss of atmospheric HO_x occurs predominantly through reaction with NO_x, and O_3 production becomes linearly dependent on the VOC abundance but inversely proportional to NO_x (the so called VOC-limited regime).

Figure 11 shows the simulated monthly mean (11:00–15:00 CST) L_{HOx}/L_{NOx} ratios and isoprene emissions in the region surrounding the tall tower from April to September 2011. As temperatures rise during summer, isoprene emissions increase (Figures 5 and 11) and drive a pronounced seasonal shift from a springtime VOC-limited regime ($L_{HOx}/L_{NOx} < 1$) to summertime NO_x-limited conditions ($L_{HOx}/L_{NOx} \geq 1$) toward the northeast and

transitional conditions (L_{HOx}/L_{NOx} ~1) elsewhere in this region. This is then followed by a general switch back to VOC-limited conditions in fall, when air temperature drops, leaves begin to senesce, and isoprene emissions decrease dramatically (Figures 5 and 11). We also see significant spatial gradients in these chemical regime shifts, reflecting the heterogeneous land cover and isoprene fluxes in this transitional region (Figures 2 and 11). The underestimated isoprene emissions for this area indicated by the low model bias in MVK + MACR (section 5) would imply a more NO_x-limited situation than is portrayed in Figure 11. Also, the anthropogenic contribution to the PTR-MS signal at *m/z* 69 was found to account for 22% of the measured signal during summer daytime. If this in fact represents anthropogenic isoprene rather than a less-reactive interferent, this would also shift Figure 11 toward a more NO_x-limited situation. However, regardless of such issues and throughout the changing seasons, the Twin Cities urban core remains VOC-limited in the model due to high local NO_x emissions.

We see here that the NO_x- and VOC-limited chemical regimes vary not only seasonally (from summer to fall and from spring to summer) but also spatially, as controlled by the timing and the spatial distribution of isoprene emissions. Analogous spatiotemporal chemical gradients will arise in other locations where isoprene emissions show strong spatial variability. Such seasonal and spatial photochemical transitions have important implications for the design of effective O_3 control strategies in different regions and for different seasons. For example, outside of the urban core and the forests to the northeast, much of the region examined here is transitional between NO_x and VOC limitation during summer (Figure 11). Under such conditions, we can expect that as domestic NO_x emissions decline [*McDonald et al.*, 2013; *de Gouw et al.*, 2014], NO_x emission controls will become increasingly effective for controlling summertime ozone.

7. Conclusions

We presented a full year of continuous in situ measurements of isoprene and its oxidation products (MVK + MACR) from the KCMP tall tower, a site lying at the ecological transition between isoprene-emitting deciduous forests to the north and east and predominantly non-isoprene-emitting agricultural landscapes to the west and south. Based on an intercomparison with cartridge measurements and a source tracer analysis, we find that anthropogenic compounds (likely isoprene itself) make a nonnegligible contribution to the *m/z* 69 signal measured by PTR-MS at this site (22% during summer daytime). Conversely, the anthropogenic contribution to the MVK + MACR signal at *m/z* 71 is small (7% during summer). We find that isoprene mixing ratios simulated by the GEOS-Chem CTM based on the MEGANv2.1 biogenic inventory have no significant bias compared to the tall tower observations once model uncertainties related to chemistry, atmospheric mixing, and land cover are taken into account. On the other hand, a persistent low model bias (−60%) in MVK + MACR that is robust across a variety of model assumptions and configurations (−25% to −66%) suggests that isoprene emissions in the broader region (but not necessarily in the immediate vicinity of the tall tower) are underestimated. This inference is consistent with the fact that the predominant isoprene emitters are concentrated 50 km or more from the tower and also with the photochemically aged nature of the biogenic mixture that reaches the tower.

We find that isoprene emissions drive a widespread seasonal shift in this region between VOC-limited chemistry during spring and fall, and NO_x-limited or transitional conditions during summer. There are major gradients in these shifts, reflecting heterogeneous land cover and isoprene emissions in this transitional region. The chemical role that isoprene plays in this area is likely still underestimated in the model due to the inferred underprediction of regional emissions (and a possible anthropogenic contribution). Based on our model simulations, much of the region surrounding the Twin Cities (outside of the consistently VOC-limited urban core itself) is transitional between NO_x- and VOC-limited conditions during summer. Continued NO_x emission reductions should therefore become more effective at controlling ozone as this area shifts to a more NO_x-limited regime.

The 0.5° × 0.667° nested GEOS-Chem model and the MEGANv2.1 biogenic inventory demonstrate significant skill at simulating the abundance of isoprene and its oxidation products MVK + MACR, despite their short atmospheric lifetimes. However, appreciable uncertainties remain due to model resolution limitations as well as errors in land cover and meteorological input data (e.g., air temperature). BVOC emission estimates have improved dramatically since the first inventories were developed 2–3 decades ago [*Lamb et al.*, 1987; *Müller*, 1992; *Guenther et al.*, 1995]. At this time, development of high-resolution, validated land cover data and more accurate meteorological fields is a key need for future improvement. Observational studies exploiting aircraft eddy covariance measurements, tall tower platforms, and satellite measurements are also needed to provide regional-scale constraints on isoprene fluxes and the subsequent atmospheric effects.

Acknowledgments
This study was supported by the National Science Foundation (grants 0937004 and 1148951), by the Minnesota Supercomputing Institute, and by a University of Minnesota Doctoral Dissertation Fellowship. We thank Tom Nelson and Minnesota Public Radio for their logistical support at the KCMP tall tower. We thank three anonymous reviewers for thoughtful comments and suggestions. We also thank Eloïse Marais for helpful discussions. Data measured at the KCMP tall tower are available for download at http://www.atmoschem.umn.edu/data.htm.

References

Andreae, M. O., and P. Merlet (2001), Emission of trace gases and aerosols from biomass burning, *Global Biogeochem. Cycles*, *15*(4), 955–966, doi:10.1029/2000GB001382.

Arneth, A., R. K. Monson, G. Schurgers, Ü. Niinemets, and P. I. Palmer (2008), Why are estimates of global terrestrial isoprene emissions so similar (and why is this not so for monoterpenes)?, *Atmos. Chem. Phys.*, *8*(16), 4605–4620, doi:10.5194/acp-8-4605-2008.

Atkinson, R., D. Baulch, R. Cox, J. Crowley, R. Hampson, R. Hynes, M. Jenkin, M. Rossi, and J. Troe (2006), Evaluated kinetic and photochemical data for atmospheric chemistry: Volume II—Gas phase reactions of organic species, *Atmos. Chem. Phys.*, *6*(11), 3625–4055, doi:10.5194/acp-6-3625-2006.

Baasandorj, M., D. B. Millet, L. Hu, D. Mitroo, and B. J. Williams (2015), Measuring acetic and formic acid by proton-transfer-reaction mass spectrometry: Sensitivity, humidity dependence, and quantifying interferences, *Atmos. Meas. Tech.*, *8*, 1303–1321, doi:10.5194/amt-8-1303-2015.

Barkley, M. P., et al. (2011), Can a "state of the art" chemistry transport model simulate Amazonian tropospheric chemistry?, *J. Geophys. Res.*, *116*, D16302, doi:10.1029/2011JD015893.

Bey, I., D. J. Jacob, R. M. Yantosca, J. A. Logan, B. D. Field, A. M. Fiore, Q. Li, H. Y. Liu, L. J. Mickley, and M. G. Schultz (2001), Global modeling of tropospheric chemistry with assimilated meteorology: Model description and evaluation, *J. Geophys. Res.*, *106*(D19), 23,073–23,095, doi:10.1029/2001JD000807.

Boersma, K. F., D. J. Jacob, M. Trainic, Y. Rudich, I. DeSmedt, R. Dirksen, and H. J. Eskes (2009), Validation of urban NO_2 concentrations and their diurnal and seasonal variations observed from the SCIAMACHY and OMI sensors using in situ surface measurements in Israeli cities, *Atmos. Chem. Phys.*, *9*(12), 3867–3879, doi:10.5194/acp-9-3867-2009.

Borbon, A., H. Fontaine, M. Veillerot, N. Locoge, J. C. Galloo, and R. Guillermo (2001), An investigation into the traffic-related fraction of isoprene at an urban location, *Atmos. Environ.*, *35*(22), 3749–3760, doi:10.1016/S1352-2310(01)00170-4.

Brown, S. S., et al. (2013), Biogenic VOC oxidation and organic aerosol formation in an urban nocturnal boundary layer: Aircraft vertical profiles in Houston, TX, *Atmos. Chem. Phys.*, *13*(22), 11,317–11,337, doi:10.5194/acp-13-11317-2013.

Carslaw, D. C., and K. Ropkins (2012), *openair*–An R package for air quality data analysis, *Environ. Modell. Software*, *27-28*, 52–61, doi:10.1016/j.envsoft.2011.09.008.

Chameides, W., R. Lindsay, J. Richardson, and C. Kiang (1988), The role of biogenic hydrocarbons in urban photochemical smog: Atlanta as a case study, *Science*, *241*(4872), 1473–1475, doi:10.1126/science.3420404.

Chen, D., Y. Wang, M. B. McElroy, K. He, R. M. Yantosca, and P. Le Sager (2009), Regional CO pollution and export in China simulated by the high-resolution nested-grid GEOS-Chem model, *Atmos. Chem. Phys.*, *9*(11), 3825–3839, doi:10.5194/acp-9-3825-2009.

Chen, M., T. J. Griffis, J. M. Baker, J. Wood, and K. Xiao (2015), Simulating crop phenology in the Community Land Model and its impact on energy and carbon fluxes, *J. Geophys. Res. Atmos.*, *120*, 310–325, doi:10.1002/2014JG002780.

Chen, Y.-H., and R. G. Prinn (2006), Estimation of atmospheric methane emissions between 1996 and 2001 using a three-dimensional global chemical transport model, *J. Geophys. Res.*, *111*, D10307, doi:10.1029/2005JD006058.

Christian, T. J., B. Kleiss, R. J. Yokelson, R. Holzinger, P. J. Crutzen, W. M. Hao, T. Shirai, and D. R. Blake (2004), Comprehensive laboratory measurements of biomass-burning emissions: 2. First intercomparison of open-path FTIR, PTR-MS, and GC-MS/FID/ECD, *J. Geophys. Res.*, *109*, D02311, doi:10.1029/2003JD003874.

Crounse, J. D., F. Paulot, H. G. Kjaergaard, and P. O. Wennberg (2011), Peroxy radical isomerization in the oxidation of isoprene, *Phys. Chem. Chem. Phys.*, *13*(30), 13,607–13,613, doi:10.1039/c1cp21330j.

de Gouw, J. A., and C. Warneke (2007), Measurements of volatile organic compounds in the Earth's atmosphere using proton-transfer-reaction mass spectrometry, *Mass Spectrom. Rev.*, *26*(2), 223–257, doi:10.1002/mas.20119.

de Gouw, J. A., C. Warneke, T. Karl, G. Eerdekens, C. van der Veen, and R. Fall (2003), Sensitivity and specificity of atmospheric trace gas detection by proton-transfer-reaction mass spectrometry, *Int. J. Mass Spectrom.*, *223*(1–3), 365–382, doi:10.1016/S1387-3806(02)00926-0 .

de Gouw, J. A., D. D. Parrish, G. J. Frost, and M. Trainer (2014), Reduced emissions of CO_2, NO_x, and SO_2 from U.S. power plants owing to switch from coal to natural gas with combined cycle technology, *Earth's Future*, *2*(2), 75–82, doi:10.1002/2013EF000196.

Duncan, B. N., et al. (2010), Application of OMI observations to a space-based indicator of NO_x and VOC controls on surface ozone formation, *Atmos. Environ.*, *44*(18), 2213–2223, doi:10.1016/j.atmosenv.2010.03.010.

Dunlea, E. J., et al. (2007), Evaluation of nitrogen dioxide chemiluminescence monitors in a polluted urban environment, *Atmos. Chem. Phys.*, *7*(10), 2691–2704, doi:10.5194/acp-7-2691-2007.

Fiore, A. M., L. W. Horowitz, D. W. Purves, H. Levy, M. J. Evans, Y. Wang, Q. Li, and R. M. Yantosca (2005), Evaluating the contribution of changes in isoprene emissions to surface ozone trends over the eastern United States, *J. Geophys. Res.*, *110*, D12303, doi:10.1029/2004JD005485.

Fu, T.-M., D. J. Jacob, P. I. Palmer, K. Chance, Y. X. Wang, B. Barletta, D. R. Blake, J. C. Stanton, and M. J. Pilling (2007), Space-based formaldehyde measurements as constraints on volatile organic compound emissions in east and south Asia and implications for ozone, *J. Geophys. Res.*, *112*, D06312, doi:10.1029/2006JD007853.

Goldstein, A. H., and I. E. Galbally (2007), Known and unexplored organic constituents in the Earth's atmosphere, *Environ. Sci. Technol.*, *41*(5), 1514–1521, doi:10.1021/es072476p.

Goldstein, A. H., M. L. Goulden, J. W. Munger, S. C. Wofsy, and C. D. Geron (1998), Seasonal course of isoprene emissions from a midlatitude deciduous forest, *J. Geophys. Res.*, *103*(D23), 31,045–31,056, doi:10.1029/98JD02708.

Griffis, T. J., J. M. Baker, S. D. Sargent, M. Eriksson, J. Corcoran, M. Chen, and K. Billmark (2010), Influence of C_4 vegetation on $^{13}CO_2$ discrimination and isoforcing in the Upper Midwest, United States, *Global Biogeochem. Cycles*, *24*, GB4006, doi:10.1029/2009GB003768.

Guenther, A., et al. (1995), A global model of natural volatile organic compound emissions, *J. Geophys. Res.*, *100*(D5), 8873–8892, doi:10.1029/94JD02950.

Guenther, A., T. Karl, P. Harley, C. Wiedinmyer, P. I. Palmer, and C. Geron (2006), Estimates of global terrestrial isoprene emissions using MEGAN (Model of Emissions of Gases and Aerosols from Nature), *Atmos. Chem. Phys.*, *6*, 3181–3210, doi:10.5194/acp-6-3181-2006.

Guenther, A. B., X. Jiang, C. L. Heald, T. Sakulyanontvittaya, T. Duhl, L. K. Emmons, and X. Wang (2012), The Model of Emissions of Gases and Aerosols from Nature version 2.1 (MEGAN2.1): An extended and updated framework for modeling biogenic emissions, *Geosci. Model Dev.*, *5*, 1471–1492, doi:10.5194/gmd-5-1471-2012.

Harley, P. C., R. K. Monson, and M. T. Lerdau (1999), Ecological and evolutionary aspects of isoprene emission from plants, *Oecologia*, *118*(2), 109–123, doi:10.1007/s004420050709.

Helmig, D., F. Bocquet, J. Pollmann, and T. Revermann (2004), Analytical techniques for sesquiterpene emission rate studies in vegetation enclosure experiments, *Atmos. Environ.*, *38*(4), 557–572, doi:10.1016/j.atmosenv.2003.10.012.

Hu, L., D. B. Millet, M. J. Mohr, K. C. Wells, T. J. Griffis, and D. Helmig (2011), Sources and seasonality of atmospheric methanol based on tall tower measurements in the US Upper Midwest, *Atmos. Chem. Phys.*, *11*(21), 11,145–11,156, doi:10.5194/acp-11-11145-2011.

Hu, L., D. B. Millet, S. Y. Kim, K. C. Wells, T. J. Griffis, E. V. Fischer, D. Helmig, J. Hueber, and A. J. Curtis (2013), North American acetone sources determined from tall tower measurements and inverse modeling, *Atmos. Chem. Phys.*, *13*(6), 3379–3392, doi:10.5194/acp-13-3379-2013.

Hu, L., et al. (2015), Emissions of C_6-C_8 aromatic compounds in the United States: Constraints from tall tower and aircraft measurements, *J. Geophys. Res. Atmos.*, *120*, 826–842, doi:10.1002/2014JD022627.

Jacob, D. J., L. W. Horowitz, J. W. Munger, B. G. Heikes, R. R. Dickerson, R. S. Artz, and W. C. Keene (1995), Seasonal transition from NO_x- to hydrocarbon-limited conditions for ozone production over the eastern United States in September, *J. Geophys. Res.*, *100*(D5), 9315–9324, doi:10.1029/94JD03125.

Karl, T., A. Guenther, C. Lindinger, A. Jordan, R. Fall, and W. Lindinger (2001), Eddy covariance measurements of oxygenated volatile organic compound fluxes from crop harvesting using a redesigned proton-transfer-reaction mass spectrometer, *J. Geophys. Res.*, *106*(D20), 24,157–24,167, doi:10.1029/2000JD000112.

Karl, T., A. Guenther, R. J. Yokelson, J. Greenberg, M. Potosnak, D. R. Blake, and P. Artaxo (2007), The tropical forest and fire emissions experiment: Emission, chemistry, and transport of biogenic volatile organic compounds in the lower atmosphere over Amazonia, *J. Geophys. Res.*, *112*, D18302, doi:10.1029/2007JD008539.

Karl, T., P. Harley, L. Emmons, B. Thornton, A. Guenther, C. Basu, A. Turnipseed, and K. Jardine (2010), Efficient atmospheric cleansing of oxidized organic trace gases by vegetation, *Science*, *330*(6005), 816–819, doi:10.1126/science.1192534.

Karl, T., A. Hansel, L. Cappellin, L. Kaser, I. Herdlinger-Blatt, and W. Jud (2012), Selective measurements of isoprene and 2-methyl-3-buten-2-ol based on NO^+ ionization mass spectrometry, *Atmos. Chem. Phys.*, *12*(24), 11,877–11,884, doi:10.5194/acp-12-11877-2012.

Kim, S. Y., D. B. Millet, L. Hu, M. J. Mohr, T. J. Griffis, D. Wen, J. C. Lin, S. M. Miller, and M. Longo (2013), Constraints on carbon monoxide emissions based on tall tower measurements in the U.S. Upper Midwest, *Environ. Sci. Technol.*, *47*(15), 8316–8324, doi:10.1021/es4009486.

Kleinman, L. I. (1994), Low and high NO_x tropospheric photochemistry, *J. Geophys. Res.*, *99*(D8), 16,831–16,838, doi:10.1029/94JD01028.

Lamb, B., A. Guenther, D. Gay, and H. Westberg (1987), A national inventory of biogenic hydrocarbon emissions, *Atmos. Environ.*, *21*(8), 1695–1705, doi:10.1016/0004-6981(87)90108-9.

Lamsal, L. N., R. V. Martin, A. van Donkelaar, M. Steinbacher, E. A. Celarier, E. Bucsela, E. J. Dunlea, and J. P. Pinto (2008), Ground-level nitrogen dioxide concentrations inferred from the satellite-borne Ozone Monitoring Instrument, *J. Geophys. Res.*, *113*, D16308, doi:10.1029/2007JD009235.

Lin, J. T., and M. B. McElroy (2010), Impacts of boundary layer mixing on pollutant vertical profiles in the lower troposphere: Implications to satellite remote sensing, *Atmos. Environ.*, *44*(14), 1726–1739, doi:10.1016/j.atmosenv.2010.02.009.

Liu, Y. J., I. Herdlinger-Blatt, K. A. McKinney, and S. T. Martin (2013), Production of methyl vinyl ketone and methacrolein via the hydroperoxyl pathway of isoprene oxidation, *Atmos. Chem. Phys.*, *13*(11), 5715–5730, doi:10.5194/acp-13-5715-2013.

Liu, Y., M. Kuwata, B. F. Strick, F. M. Geiger, R. J. Thomson, K. A. McKinney, and S. T. Martin (2015), Uptake of epoxydiol isomers accounts for half of the particle-phase material produced from isoprene photooxidation via the HO_2 pathway, *Environ. Sci. Technol.*, *49*(1), 250–258, doi:10.1021/es5034298.

Mao, J., et al. (2010), Chemistry of hydrogen oxide radicals (HO_x) in the Arctic troposphere in spring, *Atmos. Chem. Phys.*, *10*(13), 5823–5838, doi:10.5194/acp-10-5823-2010.

Mao, J., S. Fan, D. J. Jacob, and K. R. Travis (2013), Radical loss in the atmosphere from Cu-Fe redox coupling in aerosols, *Atmos. Chem. Phys.*, *13*(2), 509–519, doi:10.5194/acp-13-509-2013.

Marais, E. A., et al. (2012), Isoprene emissions in Africa inferred from OMI observations of formaldehyde columns, *Atmos. Chem. Phys.*, *12*(14), 6219–6235, doi:10.5194/acp-12-6219-2012.

Marais, E. A., D. J. Jacob, A. Guenther, K. Chance, T. P. Kurosu, J. G. Murphy, C. E. Reeves, and H. O. T. Pye (2014), Improved model of isoprene emissions in Africa using Ozone Monitoring Instrument (OMI) satellite observations of formaldehyde: Implications for oxidants and particulate matter, *Atmos. Chem. Phys.*, *14*(15), 7693–7703, doi:10.5194/acp-14-7693-2014.

McDonald, B. C., D. R. Gentner, A. H. Goldstein, and R. A. Harley (2013), Long-term trends in motor vehicle emissions in U.S. urban areas, *Environ. Sci. Technol.*, *47*(17), 10,022–10,031, doi:10.1021/es401034z.

McLaren, R., D. L. Singleton, J. Y. K. Lai, B. Khouw, E. Singer, Z. Wu, and H. Niki (1996), Analysis of motor vehicle sources and their contribution to ambient hydrocarbon distributions at urban sites in Toronto during the Southern Ontario oxidants study, *Atmos. Environ.*, *30*(12), 2219–2232, doi:10.1016/1352-2310(95)00178-6.

Millet, D. B., D. J. Jacob, K. F. Boersma, T.-M. Fu, T. P. Kurosu, K. Chance, C. L. Heald, and A. Guenther (2008), Spatial distribution of isoprene emissions from North America derived from formaldehyde column measurements by the OMI satellite sensor, *J. Geophys. Res.*, *113*, D02307, doi:10.1029/2007JD008950.

Millet, D. B., et al. (2010), Global atmospheric budget of acetaldehyde: 3-D model analysis and constraints from in-situ and satellite observations, *Atmos. Chem. Phys.*, *10*(7), 3405–3425, doi:10.5194/acp-10-3405-2010.

Misztal, P. K., T. Karl, R. Weber, H. H. Jonsson, A. B. Guenther, and A. H. Goldstein (2014), Airborne flux measurements of biogenic isoprene over California, *Atmos. Chem. Phys.*, *14*, 10,631–10,647, doi:10.5194/acp-14-10631-2014.

Monson, R. K., R. Grote, Ü. Niinemets, and J.-P. Schnitzler (2012), Modeling the isoprene emission rate from leaves, *New Phytol.*, *195*(3), 541–559, doi:10.1111/j.1469-8137.2012.04204.x.

Monson, R. K., R. T. Jones, T. N. Rosenstiel, and J.-P. Schnitzler (2013), Why only some plants emit isoprene, *Plant Cell Environ.*, *36*(3), 503–516, doi:10.1111/pce.12015.

Montzka, S. A., M. Trainer, P. D. Goldan, W. C. Kuster, and F. C. Fehsenfeld (1993), Isoprene and its oxidation products, methyl vinyl ketone and methacrolein, in the rural troposphere, *J. Geophys. Res.*, *98*(D1), 1101–1111, doi:10.1029/92JD02382.

Müller, J. F., T. Stavrakou, S. Wallens, I. De Smedt, M. Van Roozendael, M. J. Potosnak, J. Rinne, B. Munger, A. Goldstein, and A. B. Guenther (2008), Global isoprene emissions estimated using MEGAN, ECMWF analyses and a detailed canopy environment model, *Atmos. Chem. Phys.*, *8*(5), 1329–1341, doi:10.5194/acp-8-1329-2008.

Müller, J.-F. (1992), Geographical distribution and seasonal variation of surface emissions and deposition velocities of atmospheric trace gases, *J. Geophys. Res.*, *97*(D4), 3787–3804, doi:10.1029/91JD02757.

Myneni, R. B., et al. (2007), Large seasonal swings in leaf area of Amazon rainforests, *Proc. Natl. Acad. Sci. U.S.A.*, *104*, 4820–4823, doi:10.1073/pnas.0611338104.

National Research Council (1991), *Rethinking the Ozone Problem in Urban and Regional Air Pollution*, 524 pp., The National Academies Press, Washington, D. C.

Oleson, K. W., et al. (2010), Technical description of version 4.0 of the Community Land Model (CLM), *NCAR Tech. Note NCAR/TN-478+STR*, doi:10.5065/D6FB50WZ.

Olivier, J. G. J., and J. J. M. Berdowski (2001), Global emission sources and sinks, in *The Climate System*, edited by J. Berdowski, R. Guicherit, and B. J. Heij, pp. 33–78, A.A. Balkema Publishers/Swets & Zeitlinger Publishers, Lisse, Netherlands.

Palmer, P. I., D. J. Jacob, A. M. Fiore, R. V. Martin, K. Chance, and T. P. Kurosu (2003), Mapping isoprene emissions over North America using formaldehyde column observations from space, *J. Geophys. Res.*, *108*(D6), 4180, doi:10.1029/2002JD002153.

Palmer, P. I., et al. (2006), Quantifying the seasonal and interannual variability of North American isoprene emissions using satellite observations of the formaldehyde column, *J. Geophys. Res.*, *111*, D12315, doi:10.1029/2005JD006689.

Park, C., G. W. Schade, and I. Boedeker (2011), Characteristics of the flux of isoprene and its oxidation products in an urban area, *J. Geophys. Res.*, *116*, D21303, doi:10.1029/2011JD015856.

Parrella, J. P., et al. (2012), Tropospheric bromine chemistry: Implications for present and pre-industrial ozone and mercury, *Atmos. Chem. Phys.*, *12*(15), 6723–6740, doi:10.5194/acp-12-6723-2012.

Paulot, F., J. D. Crounse, H. G. Kjaergaard, J. H. Kroll, J. H. Seinfeld, and P. O. Wennberg (2009a), Isoprene photooxidation: New insights into the production of acids and organic nitrates, *Atmos. Chem. Phys.*, *9*(4), 1479–1501, doi:10.5194/acp-9-1479-2009.

Paulot, F., J. D. Crounse, H. G. Kjaergaard, A. Kürten, J. M. St. Clair, J. H. Seinfeld, and P. O. Wennberg (2009b), Unexpected epoxide formation in the gas-phase photooxidation of isoprene, *Science*, *325*(5941), 730–733, doi:10.1126/science.1172910.

Peeters, J., T. L. Nguyen, and L. Vereecken (2009), HO_x radical regeneration in the oxidation of isoprene, *Phys. Chem. Chem. Phys.*, *11*, 5935−5939, doi:10.1039/B908511D.

Pierotti, D., S. C. Wofsy, D. Jacob, and R. A. Rasmussen (1990), Isoprene and its oxidation products: Methacrolein and methyl vinyl ketone, *J. Geophys. Res.*, *95*(D2), 1871–1881, doi:10.1029/JD095iD02p01871.

Rivera-Rios, J. C., et al. (2014), Conversion of hydroperoxides to carbonyls in field and laboratory instrumentation: Observational bias in diagnosing pristine versus anthropogenically-controlled atmospheric chemistry, *Geophys. Res. Lett.*, *41*, 8645–8651, doi:10.1002/2014GL061919.

Russell, A. R., L. C. Valin, and R. C. Cohen (2012), Trends in OMI NO_2 observations over the United States: Effects of emission control technology and the economic recession, *Atmos. Chem. Phys.*, *12*, 12,197–12,209, doi:10.5194/acp-12-12197-2012.

Sasaki, K., T. Saito, M. Lämsä, K.-M. Oksman-Caldentey, M. Suzuki, K. Ohyama, T. Muranaka, K. Ohara, and K. Yazaki (2007), Plants utilize isoprene emission as a thermotolerance mechanism, *Plant Cell Physiol.*, *48*(9), 1254–1262, doi:10.1093/pcp/pcm104.

Schnitzhofer, R., A. Wisthaler, and A. Hansel (2009), Real-time profiling of organic trace gases in the planetary boundary layer by PTR-MS using a tethered balloon, *Atmos. Meas. Tech.*, *2*, 773–777, doi:10.5194/amt-2-773-2009.

Schultz, M., L. Backman, Y. Balkanski, S. Bjoerndalsaeter, R. Brand, J. Burrows, S. Dalsoeren, M. de Vasconcelos, B. Grodtmann, and D. Hauglustaine (2007), REanalysis of the TROpospheric chemical composition over the past 40 years (RETRO)–A long-term global modeling study of tropospheric chemistry: Final Report, Jülich/Hamburg, Germany.

Sharkey, T. D., F. Loreto, and C. F. Delwiche (1991), High carbon dioxide and sun/shade effects on isoprene emission from oak and aspen tree leaves, *Plant Cell Environ.*, *14*(3), 333–338, doi:10.1111/j.1365-3040.1991.tb01509.x.

Sharkey, T. D., E. L. Singsaas, P. J. Vanderveer, and C. Geron (1996), Field measurements of isoprene emission from trees in response to temperature and light, *Tree Physiol.*, *16*(7), 649–654, doi:10.1093/treephys/16.7.649.

Sharkey, T. D., A. E. Wiberley, and A. R. Donohue (2008), Isoprene emission from plants: Why and how, *Ann. Bot.*, *101*(1), 5–18, doi:10.1093/aob/mcm240.

Shim, C., Y. Wang, Y. Choi, P. I. Palmer, D. S. Abbot, and K. Chance (2005), Constraining global isoprene emissions with Global Ozone Monitoring Experiment (GOME) formaldehyde column measurements, *J. Geophys. Res.*, *110*, D24301, doi:10.1029/2004JD005629.

Sillman, S., J. A. Logan, and S. C. Wofsy (1990), The sensitivity of ozone to nitrogen oxides and hydrocarbons in regional ozone episodes, *J. Geophys. Res.*, *95*(D2), 1837–1851, doi:10.1029/JD095iD02p01837.

Stavrakou, T., J. F. Müller, I. De Smedt, M. Van Roozendael, G. R. van der Werf, L. Giglio, and A. Guenther (2009), Global emissions of non-methane hydrocarbons deduced from SCIAMACHY formaldehyde columns through 2003–2006, *Atmos. Chem. Phys.*, *9*(11), 3663–3679, doi:10.5194/acp-9-3663-2009.

Steinbacher, M., C. Zellweger, B. Schwarzenbach, S. Bugmann, B. Buchmann, C. Ordóñez, A. S. H. Prevot, and C. Hueglin (2007), Nitrogen oxide measurements at rural sites in Switzerland: Bias of conventional measurement techniques, *J. Geophys. Res.*, *112*, D11307, doi:10.1029/2006JD007971.

Stroud, C. A., et al. (2001), Isoprene and its oxidation products, methacrolein and methylvinyl ketone, at an urban forested site during the 1999 Southern Oxidants Study, *J. Geophys. Res.*, *106*(D8), 8035–8046, doi:10.1029/2000JD900628.

van der Werf, G. R., J. T. Randerson, L. Giglio, G. J. Collatz, M. Mu, P. S. Kasibhatla, D. C. Morton, R. S. DeFries, Y. Jin, and T. T. van Leeuwen (2010), Global fire emissions and the contribution of deforestation, savanna, forest, agricultural, and peat fires (1997–2009), *Atmos. Chem. Phys.*, *10*(23), 11,707–11,735, doi:10.5194/acp-10-11707-2010.

van Donkelaar, A., R. V. Martin, A. N. Pasch, J. J. Szykman, L. Zhang, Y. X. Wang, and D. Chen (2012), Improving the accuracy of daily satellite-derived ground-level fine aerosol concentration estimates for North America, *Environ. Sci. Technol.*, *46*(21), 11,971–11,978, doi:10.1021/es3025319.

von Schneidemesser, E., P. S. Monks, V. Gros, J. Gauduin, and O. Sanchez (2011), How important is biogenic isoprene in an urban environment? A study in London and Paris, *Geophys. Res. Lett.*, *38*, L19804, doi:10.1029/2011GL048647.

Wagner, P., and W. Kuttler (2014), Biogenic and anthropogenic isoprene in the near-surface urban atmosphere–A case study in Essen, Germany, *Sci. Total Environ.*, *475*, 104–115, doi:10.1016/j.scitotenv.2013.12.026.

Wang, J.-L., C. Chew, C.-Y. Chang, W.-C. Liao, S.-C. C. Lung, W.-N. Chen, P.-J. Lee, P.-H. Lin, and C.-C. Chang (2013), Biogenic isoprene in subtropical urban settings and implications for air quality, *Atmos. Environ.*, *79*, 369–379, doi:10.1016/j.atmosenv.2013.06.055.

Wang, Y. X., M. B. McElroy, D. J. Jacob, and R. M. Yantosca (2004), A nested grid formulation for chemical transport over Asia: Applications to CO, *J. Geophys. Res.*, *109*, D22307, doi:10.1029/2004JD005237.

Warneke, C., et al. (2001), Isoprene and its oxidation products methyl vinyl ketone, methacrolein, and isoprene related peroxides measured online over the tropical rain forest of Surinam in March 1998, *J. Atmos. Chem.*, *38*(2), 167–185.

Warneke, C., et al. (2010), Biogenic emission measurement and inventories determination of biogenic emissions in the eastern United States and Texas and comparison with biogenic emission inventories, *J. Geophys. Res.*, *115*, D00F18, doi:10.1029/2009JD012445.

Warneke, C., et al. (2014), Volatile organic compound emissions from the oil and natural gas industry in the Uinta Basin, Utah: Point sources compared to ambient air composition, *Atmos. Chem. Phys.*, *14*, 10,977–10,988, doi:10.5194/acp-14-10977-2014.

Wesely, M. L. (1989), Parameterization of surface resistances to gaseous dry deposition in regional-scale numerical models, *Atmos. Environ.*, *23*(6), 1293–1304.

Yuan, B., C. Warneke, M. Shao, and J. A. de Gouw (2014), Interpretation of volatile organic compound measurements by proton-transfer-reaction mass spectrometry over the deepwater horizon oil spill, *Int. J. Mass Spectrom.*, *358*, 43–48, doi:10.1016/j.ijms.2013.11.006.

Zhang, L., D. J. Jacob, N. V. Downey, D. A. Wood, D. Blewitt, C. C. Carouge, A. van Donkelaar, D. B. A. Jones, L. T. Murray, and Y. Wang (2011), Improved estimate of the policy-relevant background ozone in the United States using the GEOS-Chem global model with 1/2° × 2/3° horizontal resolution over North America, *Atmos. Environ.*, *45*(37), 6769–6776, doi:10.1016/j.atmosenv.2011.07.054.